Materials Today Bio 31 (2025) 101477

Contents lists available at ScienceDirect

Materials Today Bio

journal homepage: www.journals.elsevier.com/materials-today-bio

Hydrogel inspired by "adobe" with antibacterial and antioxidant properties for diabetic wound healing

Zouwei Li [1], Renxin Chen [1], Zhuowen Hao [1], Yan E [1], Qi Guo, Jingfeng Li [**], Shaobo Zhu [*]

Department of Orthopedics, Zhongnan Hospital of Wuhan University, Wuhan, 430071, China

ARTICLE INFO

Keywords:
Hydrogel
Core-shell fibers
Antibacterial
Antioxidant
Diabetic wound healing

ABSTRACT

With the aging population, the incidence of diabetes is increasing. Diabetes often leads to restricted neovascularization, antibiotic-resistant bacterial infections, reduced wound perfusion, and elevated reactive oxygen species, resulting in impaired microenvironments and prolonged wound healing. Hydrogels are important tissue engineering materials for wound healing, known for their high water content and good biocompatibility. However, most hydrogels suffer from poor mechanical properties and difficulty in achieving sustained drug release, hindering their clinical application. Inspired by the incorporation of fibers to enhance the mechanical properties of "adobe," core-shell fibers were introduced into the hydrogel. This not only improves the mechanical strength of the hydrogel but also enables the possibility of sustained drug release. In this study, we first prepared core-shell fibers with PLGA (poly(lactic-co-glycolic acid)) and PCL (polycaprolactone). PLGA was loaded with P2 (Parathyroid hormone-related peptides-2), developed by our group, which promotes angiogenesis and cell proliferation. We then designed a QTG (QCS/TA/Gel, quaternary ammonium chitosan/tannic acid/gelatin) hydrogel, incorporating the core-shell fibers and the anti-inflammatory drug celecoxib into the QTG hydrogel. This hydrogel exhibits excellent antibacterial properties and biocompatibility, along with good mechanical performance. This hydrogel demonstrates excellent water absorption and swelling capabilities. In the early stages of wound healing, the hydrogel can absorb the wound exudate, maintaining the stability of the wound microenvironment. This hydrogel promotes neovascularization and collagen deposition, accelerating the healing of diabetic wounds, with a healing rate exceeding 95 % by day 14. Overall, this study provides a promising strategy for developing tissue engineering scaffolds for diabetic wound healing.

1. Introduction

With the aging population, the incidence of diabetes is continuously increasing. Diabetic wounds are common complication of diabetes, with rapidly increasing prevalence that imposes significant burdens on individuals and society [1]. Diabetic wound is caused by localized high glucose levels, which results in restricted neovascularization, bacterial infections, reduced wound perfusion, and increased reactive oxygen species, ultimately damaging the skin microenvironment [2,3]. The wound healing process typically consists of four stages: hemostasis, inflammation, tissue formation, and tissue remodeling. However, patients with diabetes remain in a prolonged inflammatory state, hindering the normal healing process [4]. Hydrogels are three-dimensional network structures with high water content that mimic the porous structure of the ECM (extracellular matrix). The wet and soft characteristics of hydrogels help prevent wound dryness and reduce friction from dressings on the wound. Additionally, hydrogels can absorb exudate from the wound, maintaining stable microenvironment [5,6]. After personalized modification, hydrogels can also exhibit good biocompatibility, antibacterial properties, vasogenesis promotion ability, collagen regeneration ability and antibacterial properties, which are conducive to promoting the process of diabetic wound healing [7–10]. However, the poor mechanical properties and uncontrolled drug release behavior of hydrogels limit their application [11] (Scheme 1).

Electrospinning is a simple and efficient technique for producing nanofibers, obtaining fibers with high porosity and excellent mechanical properties [12,13]. Coaxial electrospinning is a method for creating electrospun fibers with core-shell structure, where bioactive proteins or

* Corresponding author.
** Corresponding author.
E-mail addresses: jingfengli@whu.edu.cn (J. Li), zhushaobo2000@163.com (S. Zhu).
[1] These authors contributed equally to this work and share first authorship.

https://doi.org/10.1016/j.mtbio.2025.101477
Received 30 October 2024; Received in revised form 20 December 2024; Accepted 8 January 2025
Available online 10 January 2025

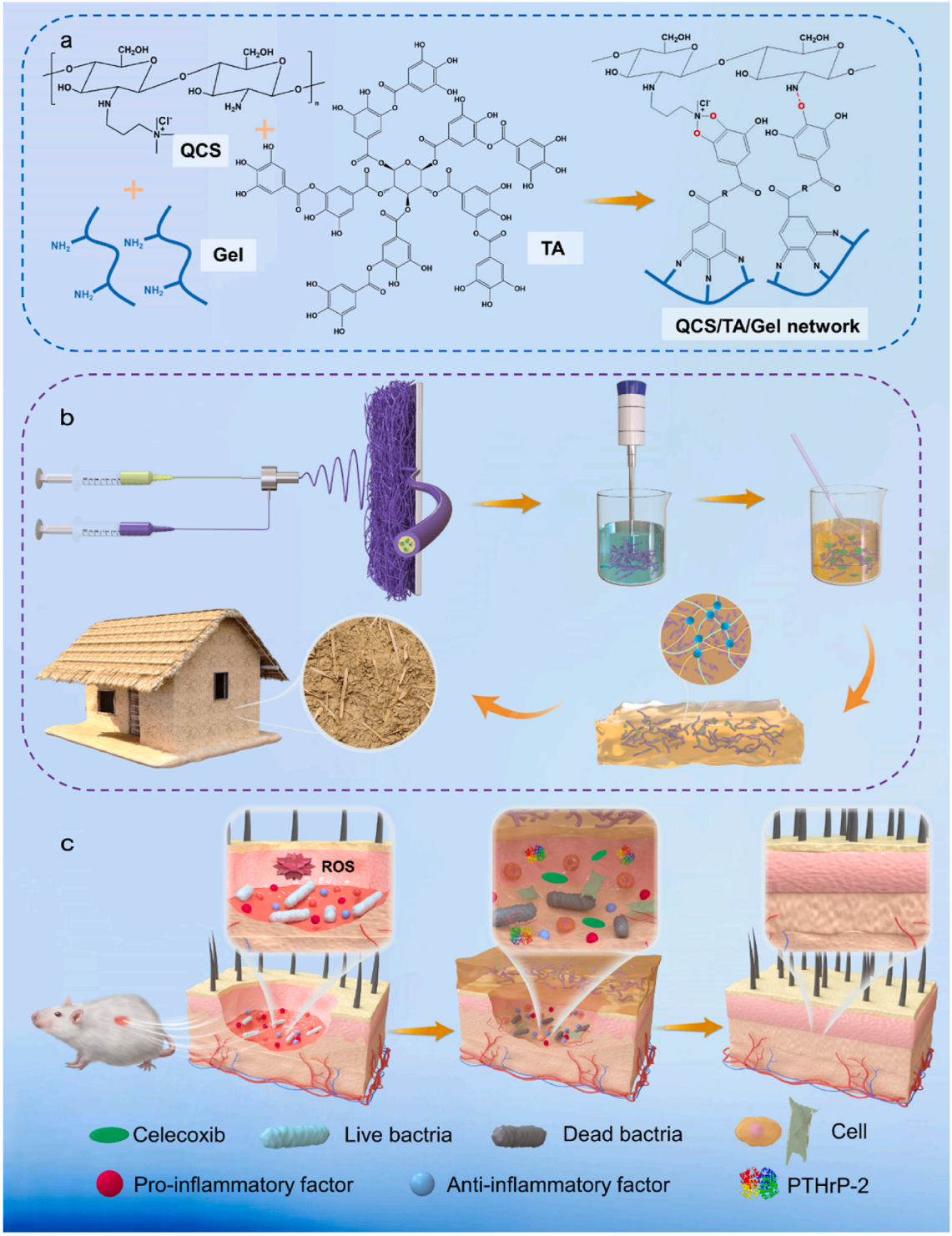

Scheme. 1. Schematic illustration of the molecular design, fabrication process, and treatment of diabetic wounds with QTG@C@PPP hydrogel. (a) Chemical structures of QCS, TA and Gel. (b) The flow chart of the hydrogel preparation. (c) The treatment process and mechanism of action of the hydrogel on diabetic wounds in rats.

drugs loaded in the core fibers are protected by the shell fibers and released in a sustained and controlled manner, achieving stable drug concentration in the local area. Coaxial electrospun fibers are thinner in diameter and exhibit better mechanical properties compared to uniaxial electrospun fiber membranes [14,15]. However, most electrospun fibers have low water content, poor shape adaptability, and may fail to maintain moisture at the wound site, thus hindering the healing process [16].

Adobe is a building material composed of sand, silt, and clay. The earliest adobe structures were made directly from raw earth, but raw earth has poor mechanical properties and low load-bearing capacity. With the continuous improvement of adobe technology, adding fibers to raw earth has become a common and effective solution. Magdaleno's research found that the compressive strength of adobe samples increased with the concentration of agave fibers, with 33 % improvement observed when 1.0 % agave fibers were added to the adobe [17].

Similarly, Ramkrishnan demonstrated that incorporating sisal fibers into adobe significantly enhanced the compressive performance of the soil [18]. The properties of hydrogels are very similar to those of adobe, as both are formed through the appropriate crosslinking of solutions. Hydrogels used as wound dressings also require good mechanical properties and the ability to be optimized by incorporating other materials. Inspired by the reinforcement of mechanical properties through the addition of fibers in adobe, this study incorporates core-shell fibers into the hydrogel. This approach not only utilizes the hydrogel's high water content and excellent biocompatibility but also combines the strong mechanical properties and drug release capabilities of the core-shell fibers. More importantly, the composite scaffold structure mimics the microstructure of proteoglycans and collagen fibers found in natural ECM, facilitating cell migration and proliferation [19].

This study first prepared core-shell fibers PPP (PLGA-PCL-P2), in which the core fiber is loaded with P2 (Parathyroid hormone-related peptides-2), developed by our research group. The fibers were then incorporated with the anti-inflammatory drug Cel (celecoxib) into QTG (QCS/TA/Gel, quaternary ammonium chitosan/tannic acid/gelatin) hydrogel to obtain the QTG@C@PPP (QCS/TA/Gel@Cel@PLGA/PCL/P2) hydrogel. QCS (quaternary ammonium chitosan) possesses a significant amount of positive charge, granting it strong antibacterial properties and tissue adhesion capabilities, as it can adsorb negatively charged bacteria through electrostatic interactions. TA (tannin acid), as a natural polyphenolic molecule, can kill bacteria by disrupting their cell membranes and inhibiting enzymatic activity, making both compounds important alternatives for non-drug antibacterial strategies [20–22]. Gel (gelatin), as a natural protein, exhibits excellent biocompatibility, adhesion, and mechanical properties [23]. PLGA, as a drug carrier, can enhance drug solubility and improve bioavailability, making it an ideal material for core fiber [24]. PCL possesses good hydrophilicity and induce no repulsion when combined with the hydrogel, while its strong mechanical properties protect PLGA [25]. P2 has been proven to promote the proliferation and migration of fibroblasts and endothelial cells, indicating its significant potential in enhancing wound healing [26,27]. Celecoxib is a COX-2 selective inhibitor that can suppress the activity of MMPs (matrix metalloproteinases) and prostaglandin E2, and the pro-inflammatory STAT3 pathway, thereby preventing delayed healing of diabetic wounds caused by inflammation. Additionally, compared to other COX-2 inhibitors, celecoxib is more stable and associated with fewer adverse effects [28,29]. According to our concept, the QTG@C@PPP hydrogel can release Cel from the hydrogel during the early stage of diabetic wound healing to achieve anti-inflammatory and antioxidant effects, while the core-shell fibers can gradually release P2 in the later stages to promote tissue repair. This approach aims to provide continuous intervention throughout the diabetic wound healing process, making it a promising candidate for a biomedicine dressing with anti-inflammatory, antibacterial, and diabetic wound healing-promoting properties.

2. Materials and methods

2.1. Materials

Quaternary ammonium chitosan (degree of substitution 95 %, 434.8 MW), Tannic acid (1701.2 MW), Sodium periodate, Sodium bicarbonate, PCL (80000 MW), Hexafluoroisopropanol was purchased from Macklin Company (Shanghai, China). Gelatin (Type A) was acquired from Beyotime Company (Shanghai, China). Sterile deionized water was obtained from Solarbio Company (Beijing, China). PLGA (60:40) was acquired from CarbonHydroTech (Guangzhou, China). tert-Butanol was purchased from Aladdin Company (Shanghai, China). Live/dead staining kit, DPPH assay kit, CCK-8 assay kit, EdU-555 assay kit, mitochondrial membrane potential assay kit (TMRE), reactive oxygen species assay kit (DCFH-DA) were acquired from Beyotime Company (Shanghai, China).

2.2. Synthesis of P2

To synthesize P2, the FMOC/tBu solid-phase method was used. The sequence consists of 1–34 amino acids of PTH with triple Glus at the C-terminus and phosphorylated Ser at the N-terminus. The full sequence of P2 is S[PO4]VSEI-QLMHN-LGKHL-NSMER-VEWLR-KKLQD-VHNF-EEE. With the assistance of BankPeptide Biological Technology Co., Ltd. (China), gel filtration was used to purify the crude peptide. To characterize the synthesis of PTHrP-2, MALDI-TOF MS (matrix-assisted laser desorption/ionization time-of-flight mass spectrometry) and HLPC (high performance liquid chromatography) were applied. The results of MALDI-TOF MS and HPLC have been confirmed by previous studies of our group [27]. The purity of P2 was $\geq$95 %, with a molecular weight of 4585.15. PTH(1–34) was obtained from Prospec (Israel).

2.3. Preparation of core-shell fibers

Firstly, PLGA was dissolved in HFIP (hexafluoroisopropanol) to prepare 20 % (w/v) PLGA solution. P2 was then added to the PLGA solution at concentration of 5 wt%, serving as the core solution for electrospinning [26]. Next, PCL was dissolved in HFIP to prepare 12 % (w/v) PCL solution, which acted as the shell solution for electrospinning. The PLGA and PCL solutions were separately drawn into 5 mL syringes and placed on a micropump, with a feed rate set at .9 mL/h. The syringes were connected via tubing to a coaxial steel needle with specification of 22G+17G, maintaining distance of 16 cm from the needle tip to the aluminum foil. The temperature and humidity were set at 25 °C and 50 %, respectively. The power supply was activated, setting the voltage to 18 kV, and the electrospinning process was conducted for 2 h. The fiber membrane was carefully removed from the aluminum foil and placed in a drying oven at 37 °C for 24 h.

2.4. Preparation of core-shell short fibers

The dried core-shell fiber membrane was cut into 1 × 1 cm squares and immersed in tert-butanol solution. The container with the fiber membrane in tert-butanol was placed in a homogenizer, set to speed of 9000 rpm for 1 h, effectively breaking the electrospun fibers into short fibers. After homogenization, the tert-butanol solution containing the short fibers was placed in a water bath at 37 °C for 24 h to allow complete evaporation of the tert-butanol, resulting in the core-shell short fibers PP/PPP (PLGA-PCL/PLGA-PCL-P2).

2.5. Preparation of QTG hydrogel

Firstly, gelatin was mixed with PP/PPP at a weight ratio of 10:1 in deionized water and stirred for 15 min to prepare 30 % gel solution containing PP/PPP short fibers. TA, QCS, sodium periodate, and Cel were each dissolved in deionized water to obtain solutions with concentrations of 2.5 % TA, 3 % QCS, .3 % sodium periodate, and 2 % Cel. Next, QCS was added to the Cel solution at a weight ratio of 20:1, resulting in a 3 % QCS solution containing Cel. The sodium periodate solution and TA solution were then mixed in a 1:1 vol ratio. This mixed solution was combined with the gel solution containing PP/PPP and the QCS solution in 2:1:1 vol ratio in a sample bottle. The pH was adjusted to 8.0 using sodium bicarbonate solution. The final solution was stirred at 37 °C for 5 min and then allowed to stand for an additional 5 min to obtain the hydrogel QTG@PP(QCS/TA/Gel@PLGA/PCL) or QTG@PPP (QCS/TA/Gel @PLGA/PCL/P2). Additionally, the mixed solution of sodium periodate and TA, along with the gel solution containing PP/PPP and the QCS solution containing Cel, was combined in 2:1:1 vol ratio in a sample bottle, with the remaining steps unchanged, resulting in the hydrogel QTG@C@PP (QCS/TA/Gel@Cel@PLGA/PCL) or QTG@C@PPP (QCS/TA/Gel@Cel@PLGA/PCL/P2). For the selection of the core-shell short fiber concentration, as shown in Fig. S1, hydrogel formation was not achieved when the concentration exceeded 3 %. This

Table 1
Materials used in preparation of hydrogels.

	Composition
QTG@PP	3%QCS+ 2.5 % TA+30 % Gel+3%PLGA-PCL fiber
QTG@C@PP	3%QCS+ 2.5 % TA+30 % Gel+ 0.15 % Celecoxib+ 3%PLGA-PCL fiber
QTG@PPP	3%QCS+ 2.5 % TA+30 % Gel+3%PLGA-PCL- P2 fiber
QTG@C@PPP	3%QCS+ 2.5 % TA+30 % Gel+ 0.15 % Celecoxib+ 3%PLGA-PCL-P2 fiber

may be attributed to excessive short fibers disrupting the hydrogel network formation. Therefore, a concentration of 3 % short fibers was selected for subsequent experiments. The composition of each hydrogel group is detailed in Table 1.

2.6. Characteristics and morphology of QTG@C@PPP

To investigate the gelation principles of the hydrogel and identify the components of the electrospun fibers, 500 mg samples of QCS, TA, Gel, Cel, and electrospun short fibers were prepared along with 500 μL of hydrogel samples. FT-IR (Fourier transform infrared spectroscopy) was performed using Nicolet iS50 (Thermo, USA) to record spectra in the range of 400–4000 cm^{-1}.

The Zeta potential was measured to determine the surface potential of the main components of the hydrogel and QTG@C@PPP. Take 5 mL of QCS, TA, and Gel solutions, and adjust the pH to 8.0. The PPP short fibers and QTG@C@PPP hydrogel were separately immersed in deionized water, homogenized for 2 h, allowed to stand for 12 h, and then the supernatant was collected for testing (Zeta Sizer Nano-25, Malvern, UK).

After stabilizing the electrospinning device, a copper grid was placed beneath the spinneret to collect the electrospun fibers. TEM (JEM-2100, JEOL, Japan) was utilized to observe the electrospun fibers on the copper grid, examining the construction of the core-shell structure.

For the preparation of 1 mL QTG@C@PPP hydrogel, once fully gelled, it was subjected to freeze-drying using a vacuum freeze dryer. The dried sample was then gold-coated and observed under SEM (Tescan VEGA Compact, TESCAN, Czech Republic) to analyze the internal microstructure of the hydrogel. EDS software was used to analyze the elemental distribution within the hydrogel, and Image J software was employed to assess the pore size distribution of the hydrogel.

2.7. Degradation performance

QTG@C@PPP was cut into small cubes measuring 20 × 20 × 20 mm and the PPP were cut into sheets measuring 20 × 20 × 5 mm. First, the initial mass of cubes and sheets m0 were measured. The cubes and sheets were then placed in centrifuge tubes containing 50 mL SBF(simulated body fluid) and incubated in a constant temperature shaker at 37 °C and 100 rpm. At regular intervals, the cubes and sheets were extracted, and surplus surface moisture was absorbed with filter paper before measuring the mass mt.

$$\text{Weight of hydrogels or electrospun fibers} = \frac{mt}{m0} \text{ x } 100\%$$

2.8. Swelling properties

QTG@C@PPP was cut into cubes measuring 20 × 20 × 20 mm, ensuring the initial hydrogel was in hydrated state. The mass of the original hydrogel (m0) was measured before fully immersing it in PBS and placing it in a 37 °C incubator. At specified time intervals, the mass (mt) was measured after gently blotting the surface moisture with filter paper. The swelling ratio of the hydrogel was calculated using the following formula:

$$\text{Swelling ratio } (\%) = \frac{mt\text{-}mo}{m0} \text{ x } 100\%$$

2.9. Water absorption properties

After freeze-drying, the initial mass of the QTG@C@PPP hydrogel was measured and recorded as m0. The hydrogel was then fully immersed in PBS and placed in a 37 °C incubator. At fixed time intervals, the hydrogel was removed, and the surface moisture was gently blotted with filter paper before measuring its mass, recorded as mt. The water absorption rate of the hydrogel was calculated using the following formula:

$$\text{Water absorption ratio } (\%) = \frac{mt\text{-}mo}{m0} \text{ x } 100\%$$

2.10. P2 and Cel release of QTG@C@PPP in vitro

To evaluate the release efficacy of P2 and Cel from QTG@C@PPP, the hydrogel was cut into 20 × 20 × 20 mm cubes and placed in a dialysis bag, which was then immersed in PBS containing 1 % Tween 20. The assembly was incubated in a shaking incubator at 37 °C (80 rpm). At designated time intervals, 1 mL the solution was withdrawn and replaced with 1 mL fresh PBS. The P2 concentration was assessed using PTH(1–34) ELISA kit (Santa Cruz, USA). And the Cel concentration was assessed using Celecoxib ELISA kit (Neogen,USA). Optical density values were measured at 450 nm using a spectrophotometric microplate reader (BioRad 680, USA) to determine the P2 and Cel concentration, and the release curves were plotted accordingly.

2.11. Rheological properties

Prepare QTG@C@PPP samples with height of 15 mm and radius of 20 mm. Place the samples on the rotating rheometer stage and assess the rheological properties using a rotational rheometer. The parameters of the rotational rheometer were set as follows: dynamic oscillatory frequency: 1–100 Hz, strain: 1 %, temperature: 37 °C. Measure and record the elastic modulus of the hydrogels after testing.

2.12. Mechanical properties

To investigate the compressive properties of QTG@C@PPP, cylindrical samples with diameter of 15 mm and height of 20 mm were prepared. An electronic universal testing machine (CMT6103, MTS, China) was utilized to apply downward compressive load to hydrogels with and without electrospun short fibers at rate of 10 mm/min, continuing until 70 % deformation was reached. The samples were then raised at rate of 20 mm/min to restore their original shape, and the results were used to plot the stress-strain curve.

To assess the tensile properties of QTG@C@PPP, samples measuring 60 × 20 × 20 mm were prepared. Each sample was positioned at the joint, and the joint angle was adjusted (45°, 60°, 90°) to observe whether the hydrogel undergoes any rupture due to deformation. Subsequently, an electronic universal testing machine (CMT6103, MTS, China) was employed to measure the stress-strain curve of the hydrogel.

2.13. Adhesive properties, injectability and transparency

Prepare sheet-like QTG@C@PPP samples and observe the adhesive effect of the hydrogel on non-biological tissues (paper, metal, plastic, glass, rubber) and biological tissues (heart, liver, spleen, lung, kidney).

Load the prepared QTG@C@PPP hydrogel solution into a 1 mL syringe before gelation. After the hydrogel has fully gelled, extrude it through the needle at a constant rate. Observe whether the structure of QTG@C@PPP is damaged and if the gel can change its ejection point according to the needle direction.

To observe the transparency of QTG@C@PPP and detect the presence of impurities, place the fully gelled QTG@C@PPP on white paper and observe if the text on the paper can be clearly seen through the

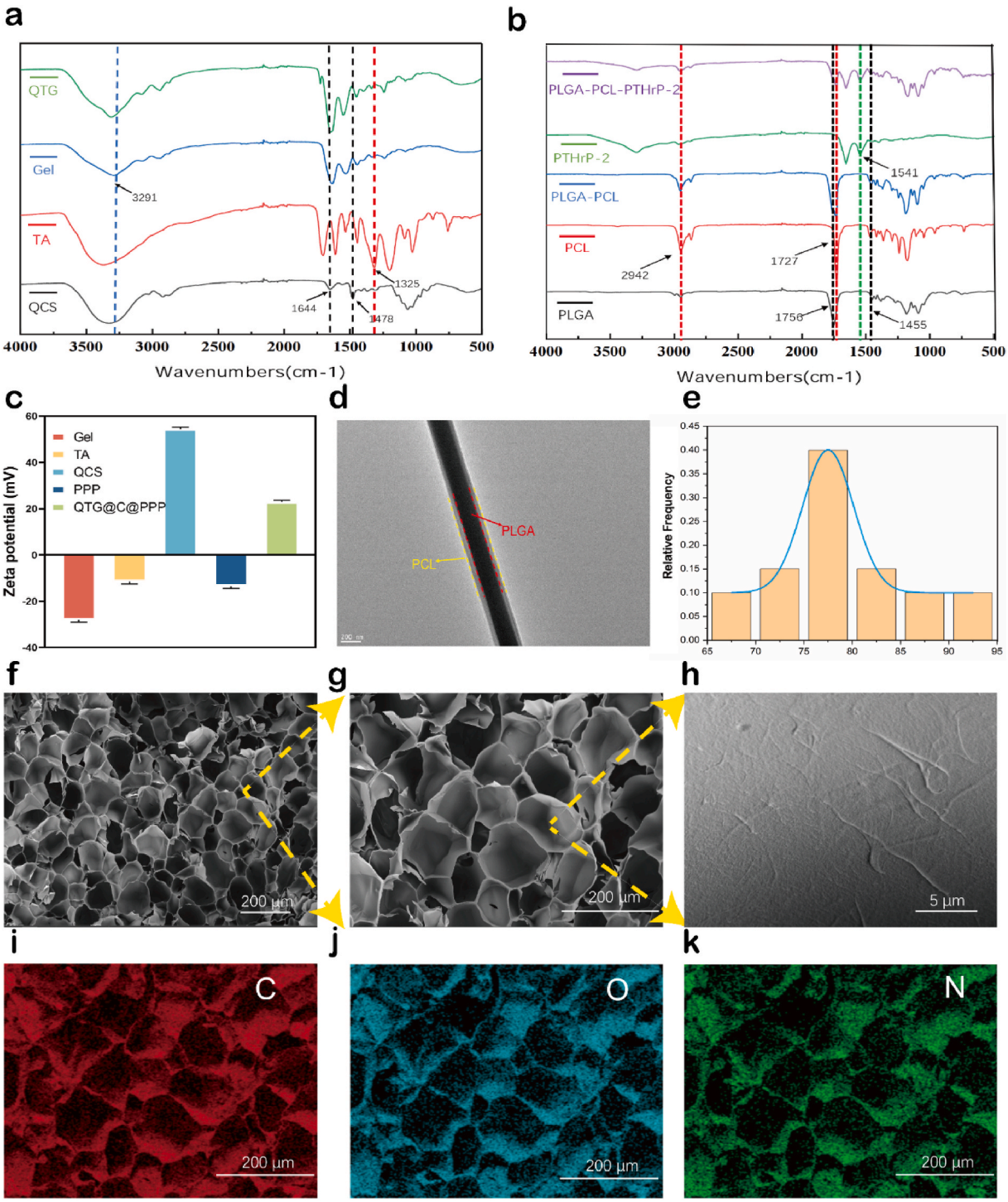

Fig. 1. Formation and mechanism of QTG@C@PPP. (a) and (b) FT-IR spectra of the QTG hydrogel and PPP electrospun fibers. (c) Zeta potential of QTG@C@PPP. (d) TEM image of the PPP electrospun fibers. (e) Pore size distribution analysis for (f). (f)–(h) SEM images of the QTG@C@PPP at magnifications of 100x, 200x, and 5000x. (i)–(k) EDS elemental analysis of (g).

hydrogel.

2.14. Antibacterial properties

To evaluate the antibacterial performance of QTG@C@PPP in vitro, *S. aureus*, *E. coli*, and *MRSA* were selected as model microorganisms. All strains were provided by the China Center for Type Culture Collection (CCTCC) at Wuhan University (Wuhan, China). In addition to the hydrogel groups, a blank group and antibiotic groups were added as controls. The blank group serves as the negative control to represent bacterial growth in the absence of hydrogel or antibiotic intervention. When calculating the antibacterial rate, the results of the blank group will be used as the denominator. PIP (piperacillin) and VAN (vancomycin) were selected as the positive control to assist in evaluating the antibacterial properties of the hydrogel groups.

Firstly, the inhibition zone method was conducted. The sterilized hydrogels were cut into 20 × 20 × 20 mm cubes and placed in LB liquid medium. Sterile paper discs were soaked in the medium to absorb the

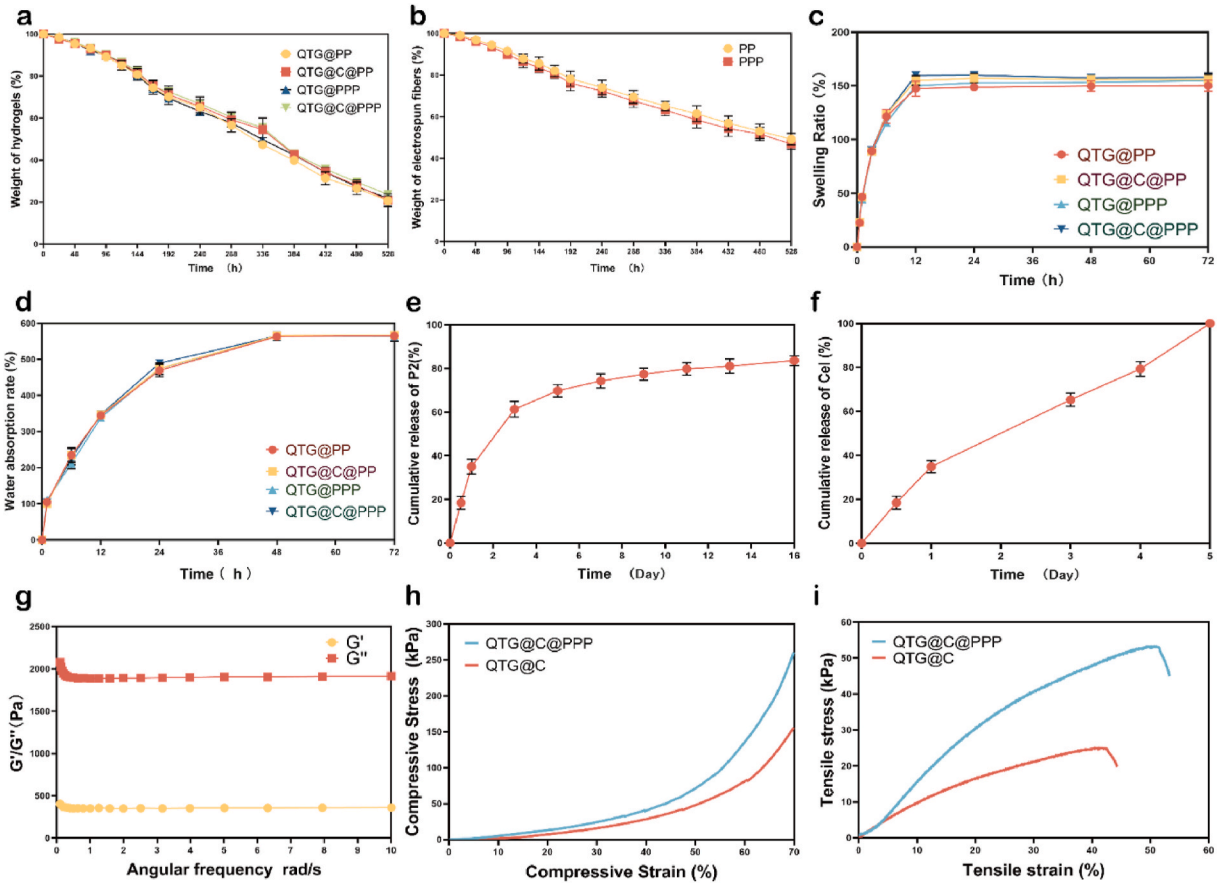

Fig. 2. Characterization of QTG@C@PPP. (a) Degradation behavior of hydrogels in vitro. (b) Degradation behavior of electrospun fibers in vitro. (c) Swelling behavior. (d) Water absorption performance. (e) P2 in vitro release. (f) Cel in vitro release. (g) Rheological properties. (h) Compressive stress-strain curve. (i) Tensile stress-strain curve.

hydrogels extract for 72 h 100 μL *S. aureus*, *E. coli*, and *MRSA* suspensions (10^6 CFU/mL) were then evenly inoculated onto LB agar plates. The paper discs with hydrogels extract were placed on different areas of the LB agar surface and incubated at 37 °C for 24 h. Photographs were taken to record the results.

Next, the plate coating method was performed and the OD600 values of the bacterial solution were measured. Bacteria were diluted to concentration of 1×10^6 CFU/ml with .9 % saline. Hydrogels cubes (20*20*20 mm) were placed in sterile tubes containing 5 mL of bacterial suspension and incubated together at 37 °C for 24 h. Bacterial suspensions (100 μL) from each group were evenly plated onto solid media, incubated at 37 °C for 24 h in biochemical incubator, and colony counts were observed and recorded. The blank group was denoted as A0 and the experimental group as A1. The OD600 absorbance of each group's bacterial suspension was measured at 600 nm at 24 and 72 h.

$$\text{Antibacterial ratio } (\%) = \frac{\text{A0-A1}}{\text{A0}} \text{ x } 100\%$$

2.15. Preparation of hydrogels extract

To conduct cell experiments, each group of hydrogels was cut into small cubes measuring 20*20*20 mm. These cubes were then soaked in DMEM culture medium containing 10 % FBS for 72 h. The hydrogel extract was used to culture cells to achieve the desired intervention effect. For the blank group, cells were directly cultured in DMEM culture medium containing 10 % FBS.

2.16. Cell acquisition and culture

L929 and HUVEC cells were obtained from the Cell Bank of the Shanghai Institute of Biochemistry and Cell Biology, Chinese Academy of Sciences (Shanghai, China). Both cell types were cultured in DMEM (Gibco, Australia) supplemented with 10 % FBS (Gibco, Australia), 100 U/mL penicillin (Thermo Fisher, USA), and 100 μg/mL streptomycin (Thermo Fisher, USA). All cells were maintained in humidified incubator at 37 °C with 5 % CO2.

2.17. Antioxidant properties

To investigate the protective effect of QTG@C@PPP against oxidative stress in cells, the number of 8×10^3 L929 and HUVEC cells were co-cultured with the hydrogel extract and H_2O_2. The Blank group was treated directly with 1 mM H_2O_2 in DMEM culture medium. After 20 min of incubation with DCFH-DA, images were captured using fluorescence microscope (Olympus IX73, Japan).

To further evaluate the antioxidant capacity of QTG@C@PPP, its ability to scavenge DPPH free radicals was assessed. A total of 400 μL QTG@C@PPP is prepared in a 24-well plate and soaked in 1 mL of anhydrous ethanol. Subsequently, 100 μL DPPH solution (dissolved in .5 mM ethanol) was added, and the mixture was incubated in the dark for 1 h. In the control group, 400 μL of DIW was used instead of the hydrogel. The absorbance of the reaction mixture was measured at 515 nm, with the absorbance of QTG@C@PPP recorded as O1 and that of the control group recorded as O2. The DPPH free radical scavenging effect of the hydrogel was calculated using the following formula:

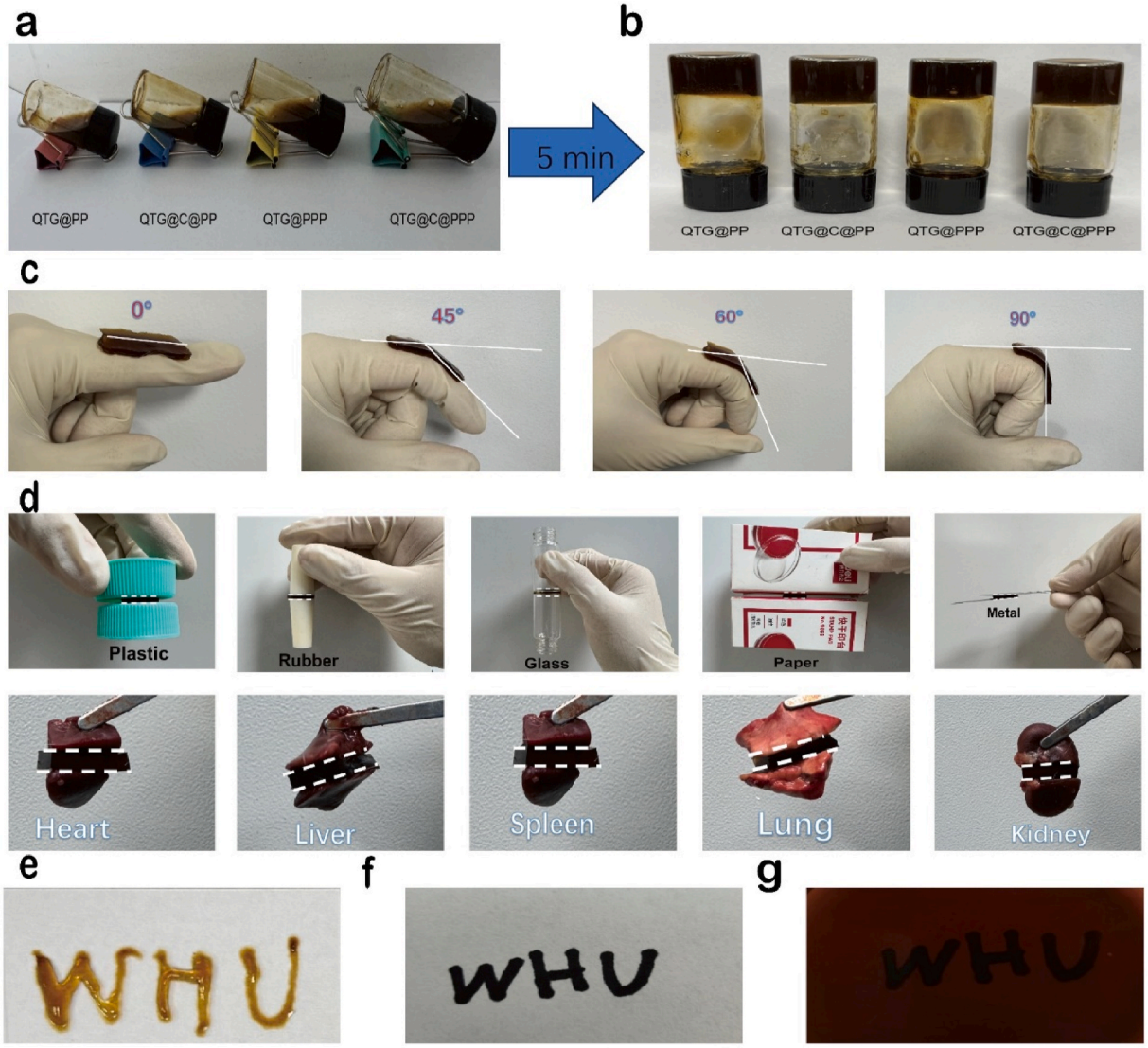

Fig. 3. Characterization of QTG@C@PPP. (a) and (b) Macroscopic views of the hydrogel. (c) Photographs of the hydrogel under tensile stretching at different angles. (d) Photographs demonstrating the adhesion of the hydrogel to various materials(The white dashed lines indicate QTG@C@PPP). (e) Images demonstrating the injectability of the hydrogel. (f) and (g) Images demonstrating the transparency of the hydrogel.

$$\text{Scavenging Effect } (\%) = \frac{\text{O2-O1}}{\text{O2}} \text{ x } 100\%$$

2.18. Biocompatibility

The biocompatibility of QTG@C@PPP was first evaluated using the CCK-8 assay. The number of 3×10^3 cells were incubated for 24 h, after which the original culture medium was replaced with the extract from each hydrogel group. The cells were then cultured for 1, 3, and 5 days. At specified time points, 100 μL CCK-8 detection reagent was added, and the cells were incubated for an additional 2 h. The OD value of each well was measured at 450 nm using a microplate reader.

To observe cell morphology, Live/dead cell staining was performed. After incubating 3×10^3 cells with the extract for 72 h, the prepared Calcein/PI staining solution was added to the 24-well plate. The plate was then incubated at 37 °C for 30 min. Cell viability was assessed using an inverted fluorescence microscope, and the percentage of viable cells was calculated.

2.19. Cell proliferation activity

The EdU cell proliferation kit was employed to assess the proliferation activity of cells following intervention with the QTG@C@PPP. The number of 5×10^3 cells were cultured with the extract from each hydrogel group for 72 h, after which staining was performed according to the manufacturer's instructions. The nuclei of proliferating cells were labeled with EdU, while all cell nuclei were stained with Hoechst 33342. The number of EdU-positive cells was observed under a fluorescence microscope, and ImageJ software was used for analysis to calculate the cell proliferation rate, defined as the number of nuclei in the proliferative phase divided by the total number of nuclei.

2.20. Cell migration ability

The Transwell assay was utilized to evaluate the impact of QTG@C@PPP on cell migration ability. The number of 5×10^3 cells were seeded in Transwell chambers with an 8 μm pore size (Corning, USA), and the hydrogel extract was added to the lower chamber. After a 12-h incubation, the cells that migrated to the lower chamber were fixed with 4 % paraformaldehyde and stained with .5 % crystal violet

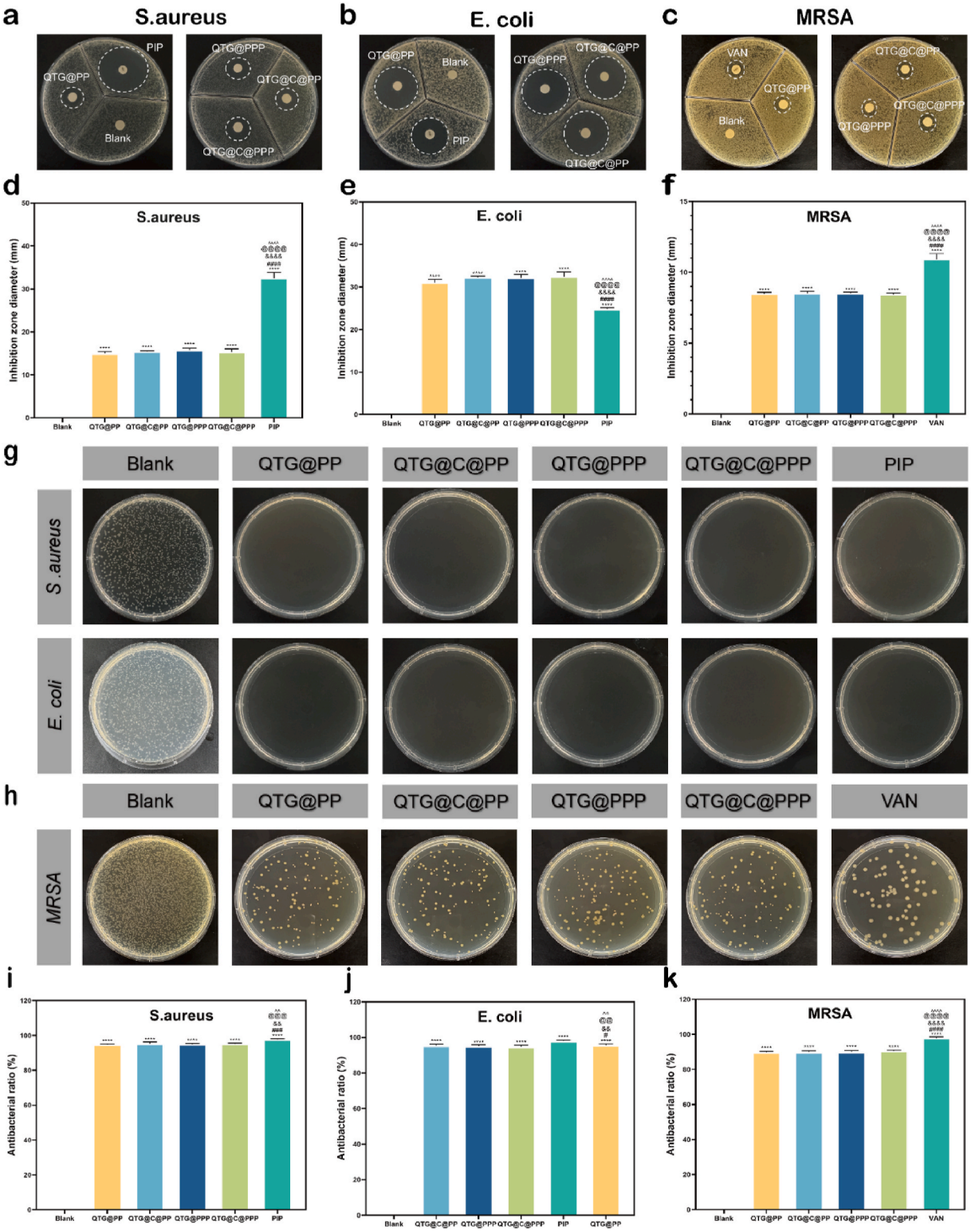

Fig. 4. Antibacterial properties of QTG@C@PPP. (a), (b) and (c) Images from the inhibition zone measurement showing the effects of the hydrogel on *S. aureus*, *E. coli*, and *MRSA*. (d), (e) and (f) Quantitative statistics from the inhibition zone measurement. (g) and (h) Images from the plate coating method for *S. aureus*, *E. coli*, and *MRSA*.(i), (j) and (k) Quantitative statistics from the plate coating method for *S. aureus*, *E. coli*, and *MRSA*.

solution. Cell morphology was then observed under an optical microscope, and the cell count was quantified using ImageJ software.

2.21. Tube formation ability

To assess the promoting effect of QTG@C@PPP on the vascular formation capability of HUVEC, tube formation assay was conducted. Firstly, the matrix gel (Corning, USA) was added to the wells using pre-cooled pipette tips. The number of 8×10^3 HUVEC that had been treated for 72 h were then placed on top of the matrix gel and cultured for 8 h. The cells were labeled with Calcein staining solution, and observations were taken using a fluorescence microscope. The parameters related to

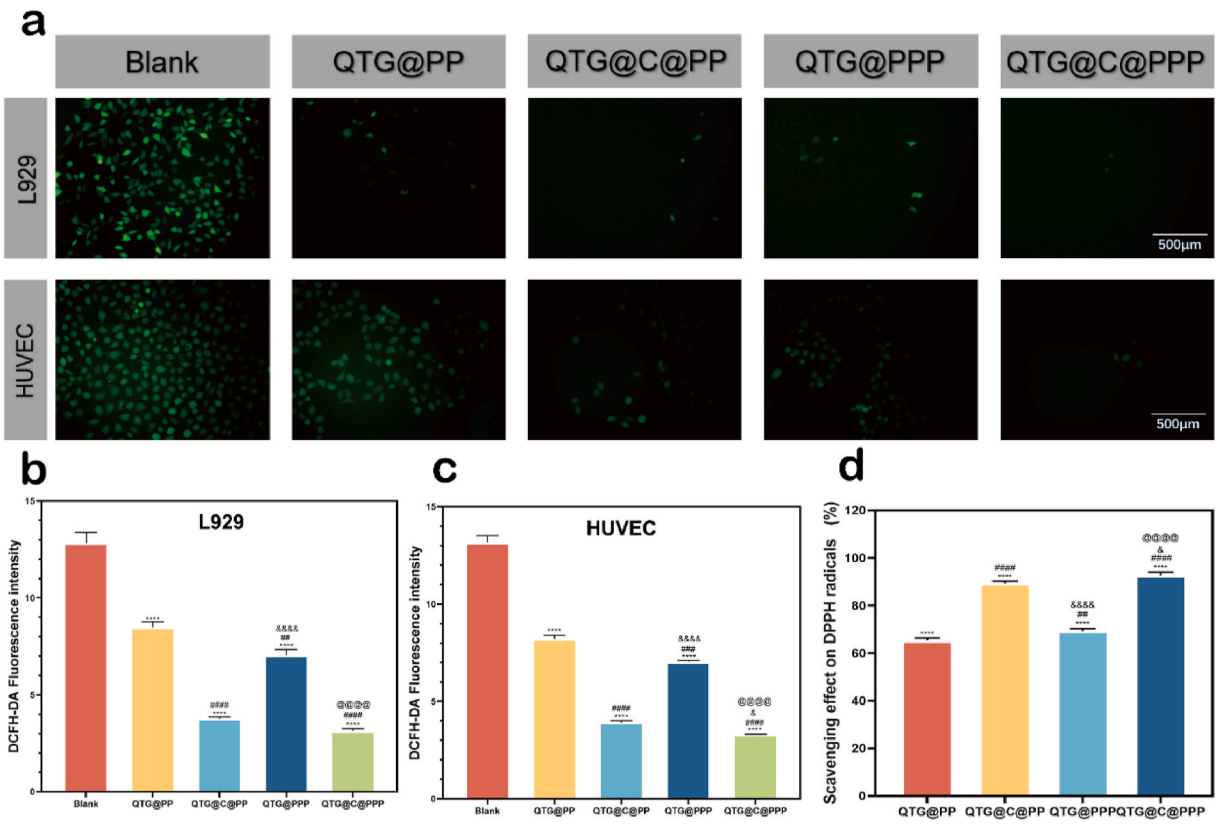

Fig. 5. Antioxidant properties of QTG@C@PPP. (a) DCFH-DA fluorescence images of cells in the presence of 1 mM H_2O_2 for each group. (b) and (c) Statistical analysis of DCFH-DA fluorescence intensity. (d) Detection of DPPH radical scavenging ability.

tube formation (number of tubes, total tube length, number of segments, and number of junctions) were calculated using Image J software along with the angiogenesis analysis plugin.

2.22. Expression analysis of wound healing-related genes

The expression changes of wound formation-related genes (VEGF, CD31, COL-1, and FGF) in HUVEC were assessed by qRT-PCR. RNA was extracted using TRIzol reagent (Invitrogen, USA). cDNA was synthesized using the RevertAid First Strand cDNA Synthesis Kit (Thermo Scientific, USA), and qRT-PCR was conducted with the ABI Prism 7300 thermal cycler (Applied Biosystems, USA) using SYBR Green detection reagent. The GAPDH gene was used to normalize the relative expression of the genes. The formula for calculating relative expression was 2−(normalized average Ct) × 100. The primer sequences are provided in Fig. S2.

2.23. Expression analysis of wound healing-related proteins

To Investigate the effect of QTG@C@PPP on wound healing-related proteins, Immunofluorescence Staining was used. The number of 5 × 10^3 HUVEC were co-cultured with the hydrogels extract for 72 h. The cells were fixed with 4 % paraformaldehyde and washed. Blocking was performed using PBS containing 3 % BSA, followed by 24 h incubation at 4 °C with primary antibodies against COL-1, VEGF, FGF, or CD31 (Proteintech, China). After washing, the cells were incubated at room temperature for 2 h with PE-labeled secondary antibodies (Bioss, China). Subsequently, the cells were incubated with Actin-Tracker Green-488/DAPI to visualize the cytoskeleton and nuclei, and observed under a fluorescence microscope.

2.24. The establishment of diabetic rat model

The animal experiment protocol and procedures involving animals were approved by the Institutional Animal Care and Use Committee (IACUC) of Wuhan University Center for Animal Experiment (Approval No. ZN2023208). All the methods were performed following the Guidelines for Animal Treatment of the Ministry of Science and Technology of the People's Republic of China. To establish diabetic models in SD rats, 1 % STZ (streptozotocin) solution was prepared using citrate buffer. 8-week-old male SD rats were fasted for 24 h, followed by a single intraperitoneal injection of STZ at dosage of 65 mg/kg. Blood glucose levels were measured continuously for 3 days after the injection, and blood glucose level ≥16.67 mmol/L confirmed the successful establishment of the diabetic rat model.

2.25. In vivo wound healing

After anesthetizing the diabetic rats, they were secured to the surgical table. The dorsal skin was shaved, and a circular wound with diameter of 25 mm was created, penetrating the full thickness of the skin. The rats were randomly divided into five groups (n = 10) and treated as follows: (1) Tegaderm^{3M}, (2) QTG@PP, (3) QTG@C@PP, (4) QTG@PPP, (5) QTG@C@PPP. The wound area was photographed on days 0, 3, 7, and 14, and the wound closure area was calculated using Image J. The wound areas on day 0 and day N were designated as A0 and AN, respectively.

$$\text{Wound area closure } (\%) = \frac{\text{A0-AN}}{\text{A0}} \text{ x } 100\%$$

2.26. Histological analysis

On days 3, 7, and 14, after anesthetizing the SD rats, tissues

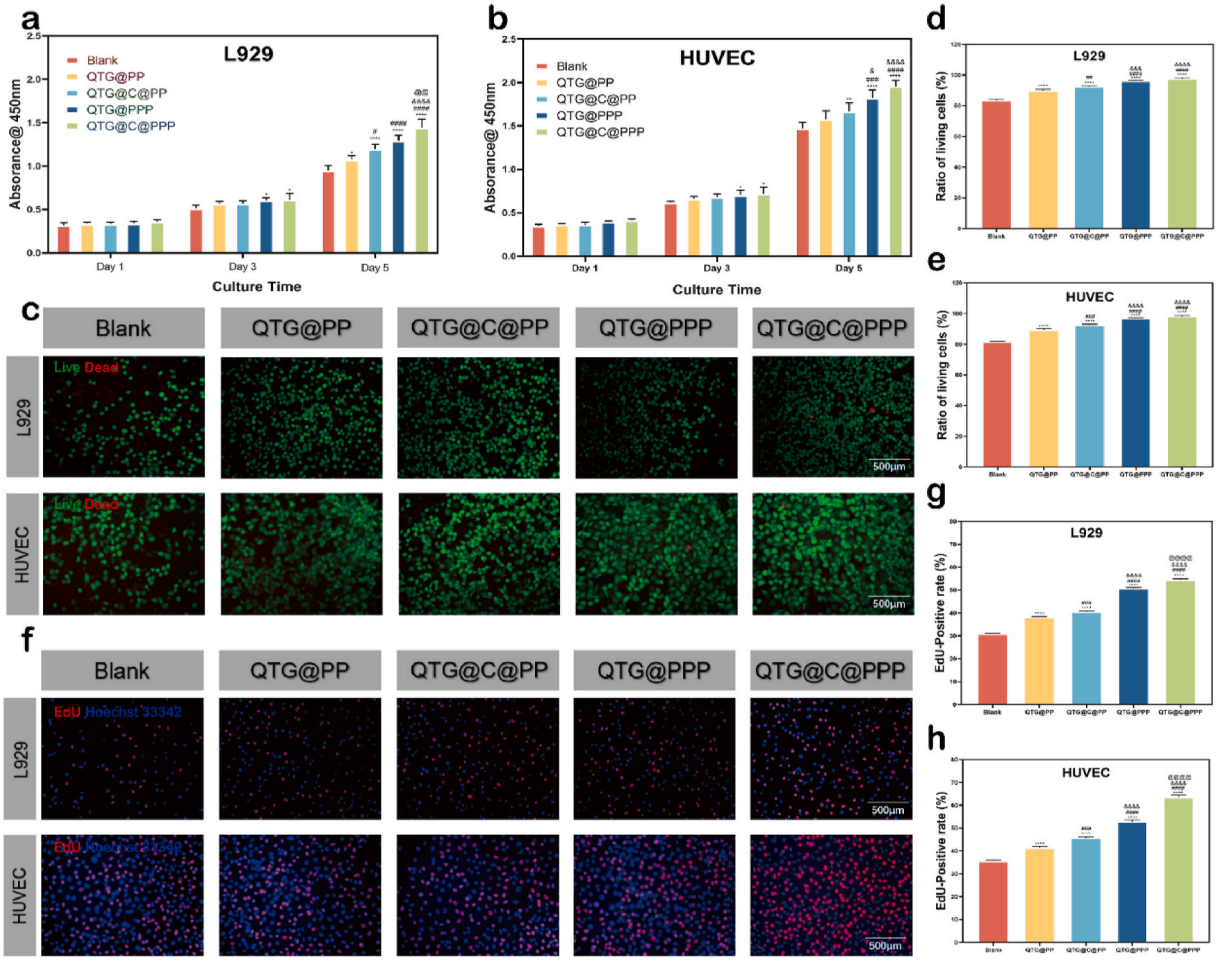

Fig. 6. Biocompatibility and cell proliferation-promoting properties of QTG@C@PPP. (a) and (b) CCK-8 results of cells on days 1, 3 and 5. (c) Live/Dead staining images of cells. (d) and (e) Statistical analysis of cell viability. (f) The images of the EdU proliferation assay for cells. (g) and (h) Statistical analysis of EdU-positive cell rates.

surrounding all skin wounds were harvested and fixed in 4 % paraformaldehyde solution. A gradient dehydration process using ethanol was performed for 30 min, followed by histological analysis using H&E staining and Masson's trichrome staining. The tissue specimens on day 14 underwent immunohistochemical staining (IL-4, IL-6, TNF-α, VEGF) to analyze local inflammation and angiogenesis at the wound site. Dehydrated and embedded sections were observed under an optical microscope (Olympus, Japan). ImageJ software was used to analyze the wound healing thickness and the collagen deposition content within the tissue.

2.27. Statistical analysis

All experiments were conducted in triplicate. Statistical analysis and quantitative image generation were performed using GraphPad Prism 8 software (GraphPad, USA). Data are presented as mean ± standard deviation. One-way analysis of variance (ANOVA) and t-tests were used to determine the statistical significance of the results.

*$p < 0.05$, **$p < 0.01$, ***$p < 0.001$ and ****$p < 0.0001$ exhibiting significant variance relative to the Blank or Tegaderm^{3M} group; #$p < 0.05$, ##$p < 0.01$, ###$p < 0.001$ and ####$p < 0.0001$ exhibiting significant variance relative to the QTG@PP group; &$p < 0.05$, && $p < 0.01$, &&& $p < 0.001$ and &&&& $p < 0.0001$ exhibiting significant variance relative to the QTG@C@PP group; @$p < 0.05$, @@ $p < 0.01$,$p < 0.001$ and @@@@$p < 0.0001$ exhibiting significant variance relative to the QTG@PPP group; ^$p < 0.05$,^^ $p < 0.01$, ^^^ $p < 0.001$ and ^^^^$p <$ 0.0001 exhibiting significant variance relative to the QTG@C@PPP group.

3. Results and discussion

3.1. Characteristics of QTG@C@PPP

FT-IR was first used to investigate the mechanism by which QCS, TA, and Gel form QTG@C@PPP. As shown in Fig. 1a, characteristic peaks representing NH_2 groups and quaternary ammonium groups appeared at 1644 and 1478 cm^{-1} for QCS. A characteristic peak for the phenolic hydroxyl group of TA was observed at 1325 cm^{-1} [30]. In the final hydrogel QTG, the two peaks of QCS were absent, and the peak for TA was significantly reduced. This may be due to the formation of ionic and hydrogen bonds between the quaternary ammonium groups or NH_2 groups of QCS and the hydroxyl groups of TA. Additionally, a characteristic peak for Gel was observed at 3291 cm^{-1} in QTG, which may result from the partial oxidation of TA's phenolic hydroxyl by sodium periodate, leading to the formation of amide bonds with the amino groups of gelatin, successfully incorporating Gel into the hydrogel [30,31]. Next, FT-IR was utilized to investigate the composition of the electrospun fibers. As seen in Fig. 1b, the characteristic peaks of the PLGA were identified at 1756 and 1455 cm^{-1} for the C=O stretch and methyl stretch, respectively. The asymmetric methylene peak for the PCL was observed at 2942 cm^{-1}, and the characteristic peak for P2 was present at 1541 cm^{-1}. These findings indicate that the core-shell fibers

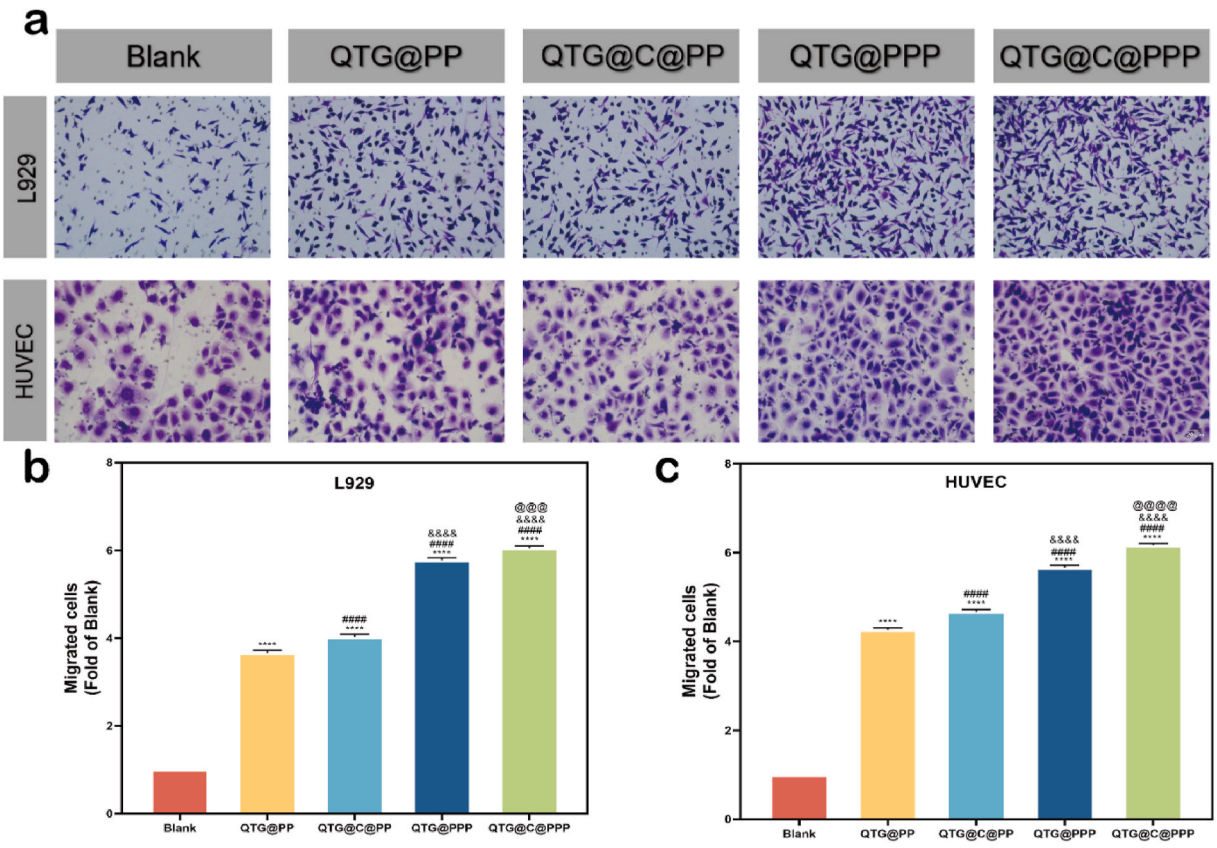

Fig. 7. The properties in promoting cell migration and protecting mitochondria of QTG@C@PPP. (a) Transwell assay images of cells. (b) and (c) Statistical analysis of migration efficiency.

PPP were successfully composed of both PLGA and PCL while also effectively loading P2 [32,33].

Subsequently, Zeta potential measurements were performed to assess the surface charge of the core-shell fibers and the components of the hydrogel. As shown in Fig. 1c, PPP exhibited a negative surface charge, while components of the hydrogel, including TA and Gel, also carried a small negative charge. In contrast, QCS displayed a significant positive surface charge, and QTG@C@PPP exhibited a positive surface charge as well. This enhanced positive charge in QCS, likely due to its higher content, may facilitate better interactions with negatively charged bacteria, improving its antibacterial properties [34].

3.2. Morphology of QTG@C@PPP

Firstly, TEM was employed to observe the PPP fibers. The fibers exhibited distinct "core-shell" structure(Fig. 1d), with continuous and uniform shell layer enveloping the core. SEM images of QTG@C@PPP (Fig. 1f-h) revealed uniformly porous hydrogel structure, with short fibers visible at high magnification. The pore size distribution of the hydrogel tended to be consistent, indicating stable microstructure (Fig. 1e). The three-dimensional porous structure of QTG@C@PPP can serve as a channel for moisture storage and exchange, simulating the architecture of the ECM and facilitating cell adhesion and migration. Moreover, EDS was utilized to measure the elemental distribution within the microstructure of QTG@C@PPP (Fig. 1i-k). The results indicated that the elements C, O, and N were uniformly distributed throughout the hydrogel. Statistical analysis revealed that the

carbon content in the hydrogel was the highest at 60.17 %, followed by oxygen at 24.05 %, and nitrogen at 15.78 % (Fig. S3). More importantly, the element N in the hydrogel is primarily provided by QCS. As shown in Fig. 1k, the element N is evenly distributed within the hydrogel, indicating that QCS forms a uniform network with other components during the gelation process.

3.3. Degradation performance

Wound dressing biomaterials need not only cover the wound for a specified period but also begin degrading at an appropriate time, preventing interference with wound regeneration and scar tissue shedding. The results of hydrogels in vitro degradation, shown in Fig. 2a, indicate that each hydrogel group retained over 50 % of its mass after 12 days of immersion in SBF, demonstrating suitability for the extended demands of diabetic wound healing [35]. Electrospun fibers PPP, as supporting component in QTG@C@PPP and carrier for P2 release, require a slower degradation time to meet the demands. As shown in Fig. 2b, after soaking PPP in SBF for 20 days, it retains 50 % of its mass, indicating that during the degradation process of QTG@C@PPP, PPP still plays a role in preventing the collapse of the hydrogel and maintaining P2 release.

3.4. Swelling, water absorption, and gelation time of hydrogels

The rate at which hydrogel reaches swelling equilibrium is a fundamental indicator of hydrogel quality. Firstly, the swelling rate of fully gelled hydrogel was tested. As shown in Fig. 2c, all hydrogels rapidly swelled over 100 % within 6 h, reaching equilibrium at 150 % by 12 h. Next, the water absorption rate of freeze-dried hydrogel was measured, as illustrated in Fig. 2d. Each hydrogel group achieved 100 % water absorption within 1 h, and by 48 h, they reached equilibrium with absorption rate exceeding 500 %. This may be due to the tightly cross-linked network of QTG@C@PPP and the hydrophilic groups on TA and Gel, which likely facilitated accelerated water absorption and shortened the time to equilibrium [36]. As shown in Fig. 3a and b, when the hydrogel components were added to sample vials and left to stand

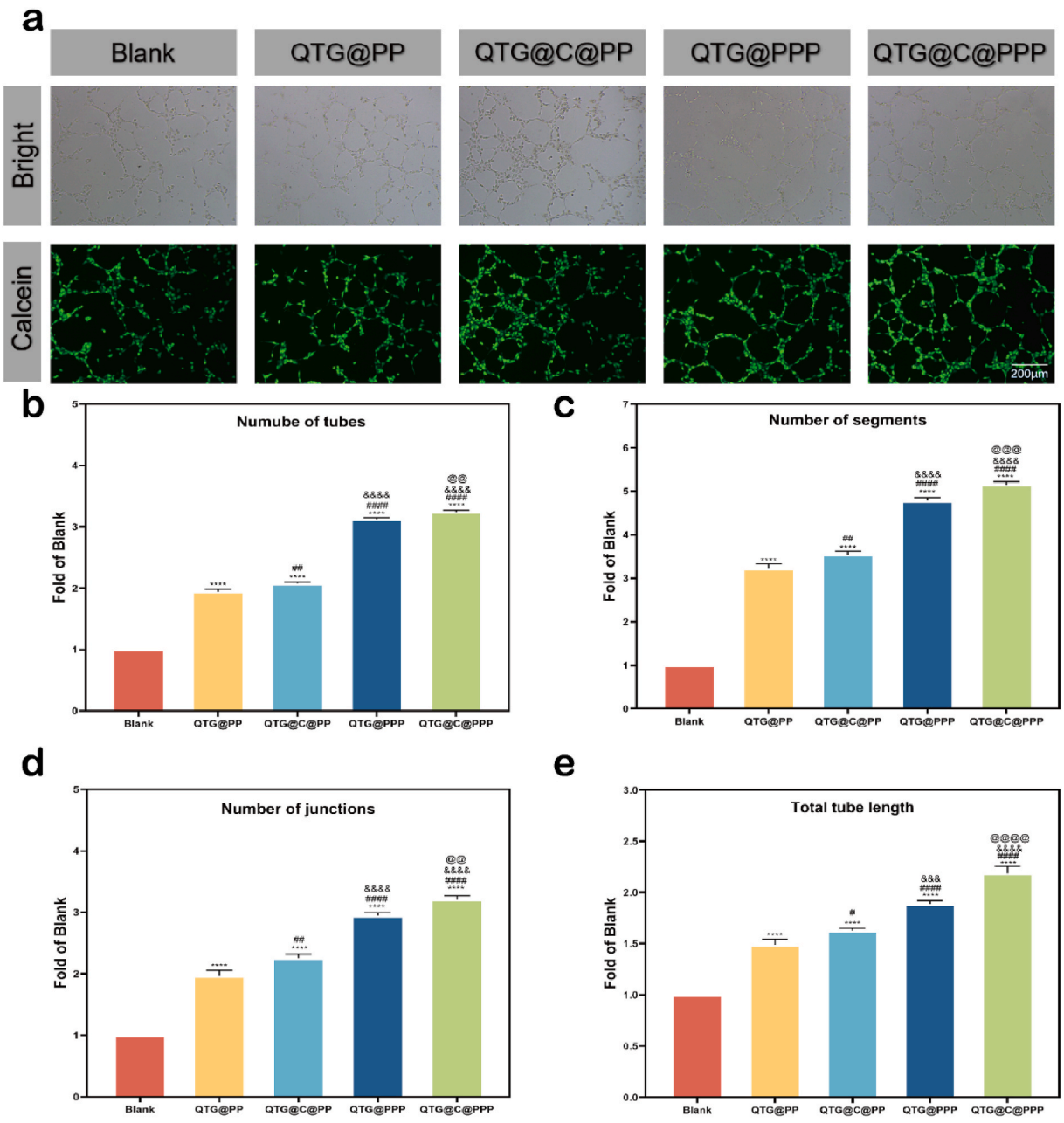

Fig. 8. The properties in promoting tube formation of QTG@C@PPP. (a) Bright-field and fluorescence images of the tube formation assay. (b) Statistical analysis of the number of tubes. (c)–(e) Statistical analysis of the total tube length, number of segments, and number of junctions in the tube formation.

for 5 min, no flow was observed upon inversion, indicating complete gelation. QTG@C@PPP not only exhibits excellent moisture retention but also has strong water absorption and rapid gelation capabilities, helping to maintain moist wound environment while quickly absorbing exudate and blood, thereby promoting diabetic wound healing.

3.5. *In vitro release of P2 and Cel*

P2 was loaded into the core layer of core-shell fibers to study the drug release behavior in vitro. As shown in Fig. 2e, the release exhibited an initial burst phase, releasing 61.3 % of the loaded amount within the first three days. Following this, the release entered a sustained phase, where P2 continued to be released from QTG@C@PPP, reaching 83.6 % cumulative release by day 16. This burst release may be attributed to occasional instability in the Taylor cone during electrospinning, causing some P2 to remain unencapsulated within the shell layer and to leak into the hydrogel matrix during preparation. As the hydrogel degraded in the initial stages, the leaked P2 was released, accounting for the initial burst. Once this unencapsulated P2 was depleted, the release transitioned to a sustained, slow phase as P2 was gradually released from the core layer fibers, ensuring early achievement of an effective drug concentration and a subsequent prolonged release to maintain it.

Cel, loaded in the hydrogel and in direct contact with the external environment, was released more rapidly. As shown in Figs. 2f and 34 % Cel was released on the first day, and it was completely released by the 5th day, with stable release profile without sudden or delayed release events. As an anti-inflammatory drug, Cel needs to reach effective local drug concentration at the diabetic wound site early to exert its anti-inflammatory and antioxidant effects. In the later stages of healing, where repair becomes the primary focus, the cessation of celecoxib release have no adverse impact.

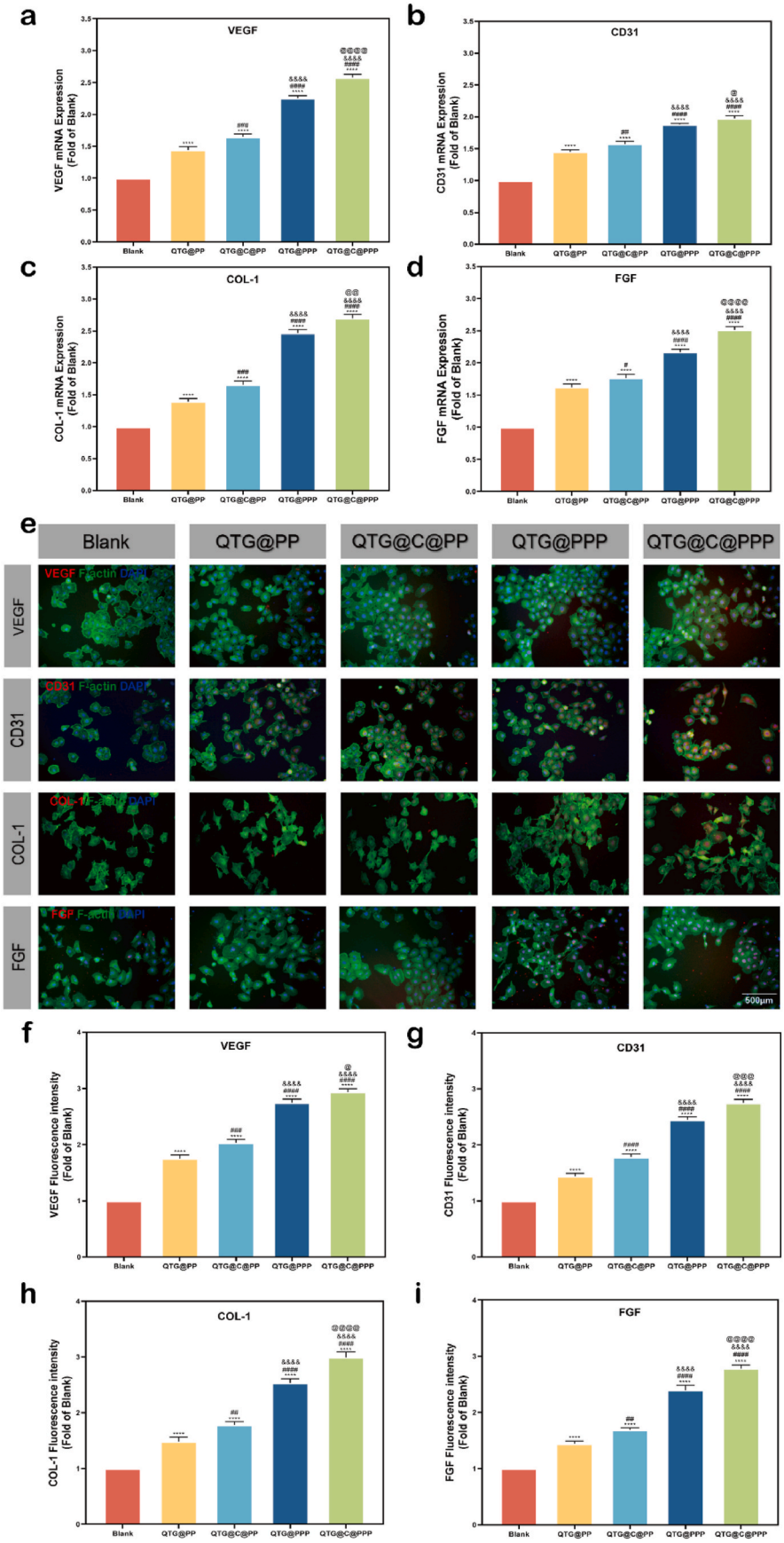

Fig. 9. The expression of COL-1, VEGF, FGF, and CD31 in HUVEC. (a)–(d) Statistical analysis of relevant genes in HUVEC using qRT-PCR. (e) The immunofluorescence staining images of relevant genes in HUVEC. (f)-(i)Statistical analysis of immunofluorescence intensity.

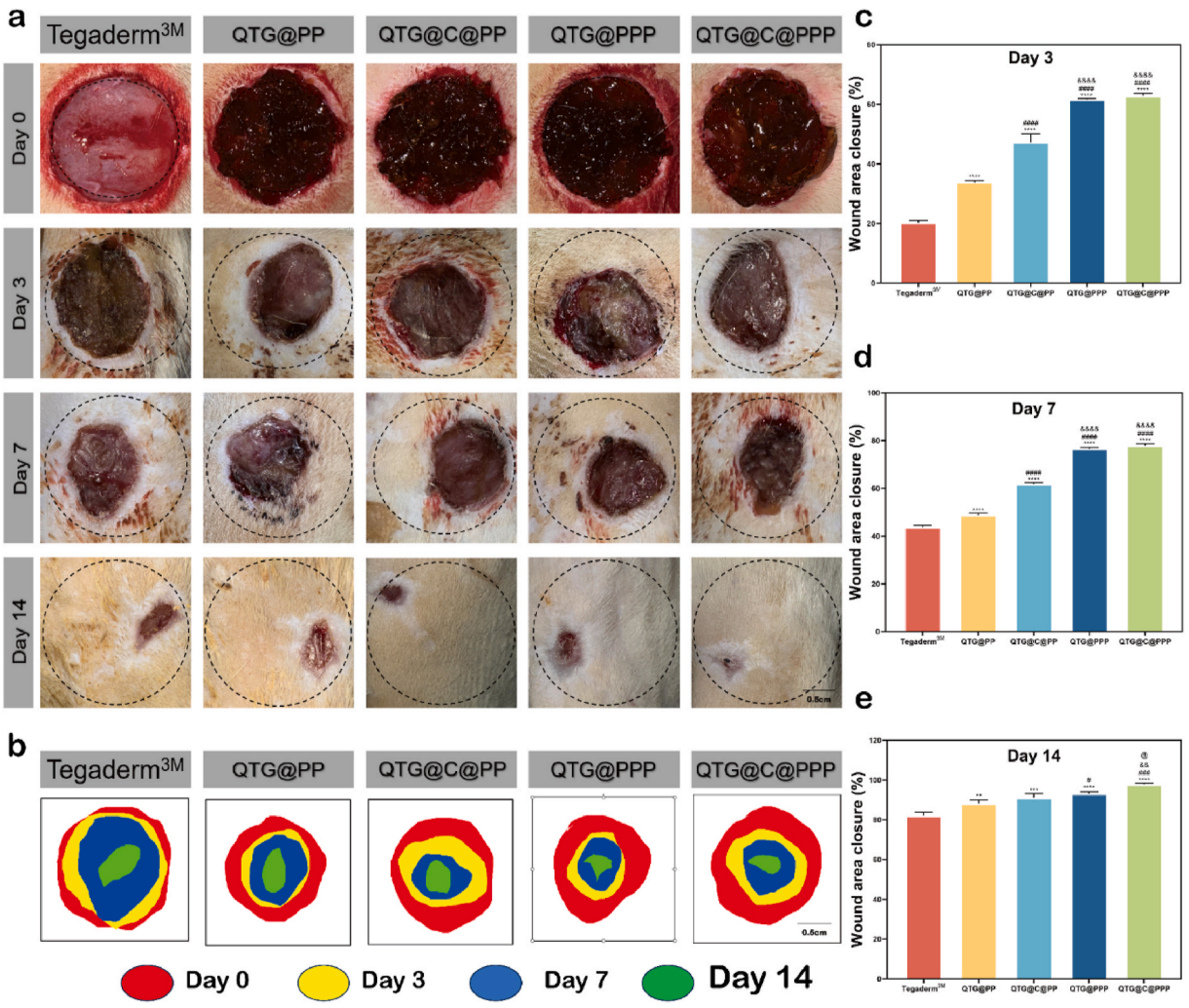

Fig. 10. In vivo assessment of QTG@C@PPP for wound healing. (a) The images of wounds at days 0, 3, 7 and 14 after different treatments. (b) Healing traces of different treatment groups at day 14. (c) -(e)Statistical analysis of wound healing rates in different treatment groups at days 3, 7 and 14.

3.6. Rheological properties

It is generally accepted that when a material behaves more like elastic solid, the storage modulus (G′) is greater than the loss modulus (G″), while a liquid-like behavior is indicated when G′ is less than G''. As shown in Fig. 2g, QTG@C@PPP consistently exhibited the storage modulus (G′) greater than the loss modulus (G″) throughout the test, indicating its elastic solid-like nature. This suggests that QTG@C@PPP maintains shape stability while also possessing some elasticity, making it suitable for use as a diabetic wound dressing.

3.7. Mechanical properties

Dressings in contact with the external environment or under pressure may crack or detach, potentially exposing the wound. Therefore, mechanical properties are essential for wound dressings, as stronger mechanical performance suggests greater application potential [37]. As shown in Fig. 2h, the compression resistance of QTG@C@PPP, containing core-shell fibers, was significantly higher than QTG@C. Neither sample was damaged at 70 % strain; however, QTG@C@PPP tolerated greater pressure.

An ideal hydrogel wound dressing should also accommodate movements at various angles without damage upon stretching. A strip-shaped hydrogel was applied to a knuckle, and as demonstrated in Fig. 3c, QTG@C@PPP deformed at specific angles (45°, 60°, and 90°) without breaking or tearing. The stress-strain curve (Fig. 2i) showed that QTG@C@PPP could withstand greater tensile force at the same strain level compared to QTG@C, more closely matching normal skin behavior. This improvement may be due to the addition of core-shell fibers, which provide structural support to the loose hydrogel matrix, creating stress concentration points under load and enhancing the compression and tensile properties of QTG@C@PPP [38].

3.8. Adhesion properties, injectability and transparency

An ideal wound dressing should adhere to the wound surface, providing a barrier against microbial infection, reducing bodily fluid leakage, and aiding in hemostasis. As shown in Fig. 3d, QTG@C@PPP could adhere to surfaces of non-biological materials and biological tissues, with sufficient adhesion strength to ensure that the hydrogel would not be easily removed. This indicates that the adhesion properties of QTG@C@PPP are similar to those of other hydrogels used for wound treatment [31]. This strong adhesion may be attributed to the mucosal adhesiveness of QCS and the general adhesiveness of TA, while Gel also contributes to the adhesive properties. Together, these components endow QTG@C@PPP with exceptional adhesive capability [39–41].

Injectable hydrogels offer the advantages of easy portability and adaptability to wound contours, allowing for personalized wound dressing. As shown in Fig. 3e, once fully gelled, QTG@C@PPP could be smoothly dispensed from a 1 mL syringe, allowing for writing on a glass

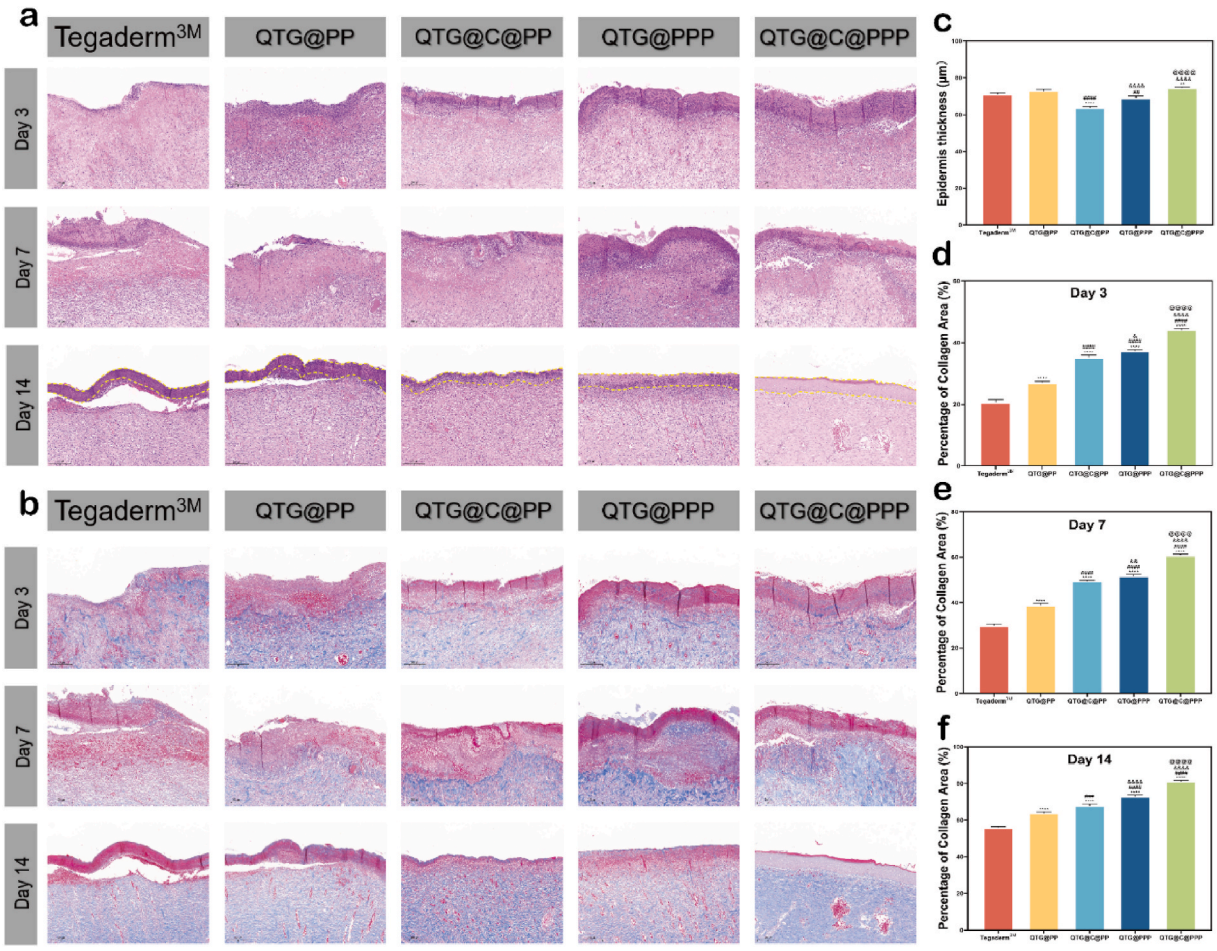

Fig. 11. Histological evaluation of wound regeneration. (a) H&E stained images of wound tissues in each group at days 3, 7 and 14. (b) Masson trichrome stained images of wound tissues in each group (at days 3, 7, and 14). (c) Statistical analysis of epithelial layer thickness at day 14 in H&E stained images (epithelial thickness indicated between two yellow dashed lines). (d)–(f) Collagen density at different time points in each group. (For interpretation of the references to colour in this figure legend, the reader is referred to the Web version of this article.)

slide without compromising the hydrogel structure. Most of the wound dressings are opaque, making it difficult to assess the healing status of the wound and determine the appropriate time to change dressings. The transparency of the hydrogel, illustrated in Fig. 3f and g, allows for clear visibility of text beneath it, with no impurities observed within the hydrogel, indicating excellent transparency. This suggests that QTG@C@PPP can be used for wound healing, allowing dynamic assessment of wound healing progress and determination of the next treatment plan without removing the dressing.

3.9. Antibacterial properties

The high-glucose microenvironment of diabetic wounds is conducive to bacterial infections, which can significantly impede healing. However, the growing burden of antibiotic resistance poses challenges for individuals and society, making dressings with inherent antimicrobial properties a superior choice for diabetic wounds [42,43]. To assess the antibacterial properties of QTG@C@PPP, the inhibition zone method was conducted. As shown in Fig. 4a–c, all hydrogel groups exhibited clear inhibition zones around the paper discs. According to statistical analysis (Fig. 4d–f), the inhibition zone diameter for *S. aureus* was approximately 15.1 mm for all hydrogel groups, slightly lower than that of PIP, which measured 32.5 mm. For *E. coli*, the hydrogel groups demonstrated an inhibition zone diameter of around 32.2 mm, outperforming PIP, which had diameter of 24.7 mm. Regarding *MRSA*, a multidrug-resistant strain, the inhibition zone diameter for the hydrogel groups was about 8.5 mm, whereas VAN showed an inhibition zone diameter of 10.9 mm, indicating that the antibacterial properties of QTG@C@PPP was slightly weaker than that of VAN.

Then, the plate coating method was used to further investigate the antibacterial properties of QTG@C@PPP (Fig. 4g and h), revealing that the number of bacterial post-treatment was significantly lower than that of the control group. Over 99 % *S. aureus* and *E. coli* were effectively killed, while the hydrogel groups exhibited 90 % inhibition rate against *MRSA*, with no statistically significant differences observed between the various hydrogel groups (Fig. 4i–k).

Finally, bacterial proliferation was analyzed using OD600 measurements (Figs. S4a–c), and all hydrogel groups showed clear inhibitory effect on bacterial growth. Specifically, the inhibition of *S. aureus* was slightly weaker than that of PIP, while the inhibition of *E. coli* was stronger than that of PIP. The inhibition against *MRSA* was also slightly weaker than that of VAN, consistent with the results from the inhibition zone test.

The antibacterial properties of QTG@C@PPP stem from the combined effects of QCS and TA. QCS carries a substantial positive charge, enabling it to adsorb negatively charged bacteria and disrupt the integrity of their cell walls. Meanwhile, the phenolic hydroxyl groups in TA exert their bactericidal effect by damaging bacterial membranes and inhibiting enzymatic activity, collectively providing robust antibacterial properties [21,44].

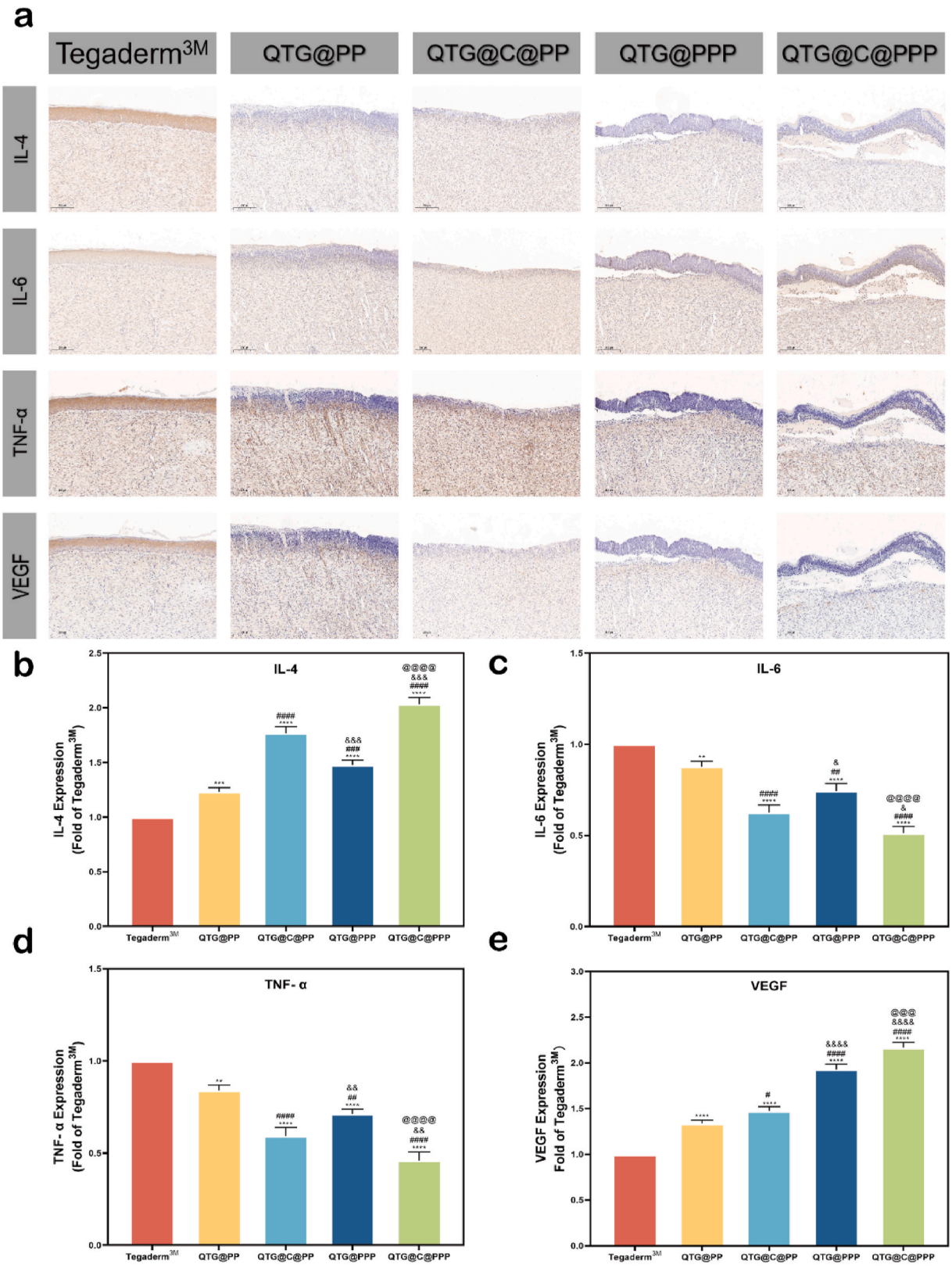

Fig. 12. Immunohistochemical analysis of regenerated wound tissue. (a) Immunohistochemical staining images of wound tissues at day 14. (b)–(e) Statistical data of the relative expression levels of inflammatory factors and vascular formation-related factors at day 14.

3.10. Antioxidant properties

ROS (Reactive oxygen species) are small molecules generated by the respiratory chain. While low levels of ROS can promote wound healing through cell-survival signaling cascades, elevated ROS levels can induce oxidative stress, leading to cellular damage, necrosis, and ultimately local inflammation. Diabetic patients often experience delayed wound healing due to increased ROS penetration resulting from reduced

antioxidant enzyme activity [45,46]. Firstly, DCFH-DA staining was used to detect the cellular response to oxidative stress after QTG@C@PPP intervention. As shown in Fig. 5a, the fluorescence intensity in cells treated with various hydrogels was significantly lower than that in the control group. Statistical analysis (Fig. 5b and c) revealed that the fluorescence intensity in the Cel-containing group was one-third of that in the Blank group and half of that in the hydrogel group without Cel.

Next, the scavenging ability of each hydrogel group against DPPH free radicals was explored. As illustrated in Fig. 5d, the hydrogel group without Cel achieved scavenging rate of 65 %, while the group containing Cel reached rate of 90 %. These results are consistent with other hydrogels with antioxidant properties, demonstrating that QTG@C@PPP possesses excellent antioxidant performance [31,47]. This may be due to the abundant ortho-hydroxyl groups in TA, which can release hydrogen to scavenge free radicals, block chain reactions, and inhibit lipid peroxidation, while Cel may reduce oxidative stress through the STAT3 pathway [48,49]. In addition, the abundant amino groups and hydroxyl groups containing active hydrogen in QCS also confer ROS scavenging ability to hydrogel, allowing TA, QCS and Cel to work synergistically in the antioxidant process [50].

3.11. Biocompatibility and cell proliferation activity

As wound dressing, good biocompatibility is essential. CCK-8 assay was used to assess the effect of QTG@C@PPP on cell viability. As shown in Fig. 6a and b, the absorbance values of L929 and HUVEC treated with the hydrogels were higher than those of the Blank group at all time points, indicating that the proliferation activity of the cells was not inhibited. The Live/dead staining (Fig. 6c) showed that most of the cells treated with QTG@C@PPP were stained green and appeared normal, with no red fluorescence observed, while the Blank group exhibited cell debris at the edges. After statistical analysis (Fig. 6d and e), the cell viability in all groups was greater than 80 %, with both QTG@PPP and QTG@C@PPP groups exceeding 95 %, indicating that P2 improved the biocompatibility of the hydrogels.

EdU staining was used to evaluate the effect of QTG@C@PPP on cell proliferation. As shown in Fig. 6f, the proportion of red fluorescence in the hydrogel groups was significantly higher than in the Blank group. Statistical analysis revealed (Fig. 6g and h) that the proliferation rates of cells in the QTG@PPP and QTG@C@PPP groups were greater than 50 %, indicating that the hydrogels significantly promoted cell proliferation. Both TA and Gel in the hydrogels can induce the production of growth factors, and P2 has been confirmed to promote cell proliferation [27,51,52]. Additionally, the inclusion of core-shell fibers provides support points for cell growth and adhesion, mimicking the structure of proteoglycans and collagen fibers in the ECM, thus facilitating cell proliferation [19].

3.12. Cell migration ability

During the wound healing process, the rapid migration of fibroblasts and endothelial cells is crucial for repair, as it allows for early coverage of the wound and provides essential nutrients, maintaining the homeostasis of the microenvironment [53]. As shown in Fig. 7a–c, the number of migrating cells in all hydrogel groups was greater than that in the Blank group over the same time period. Notably, QTG@PPP and QTG@C@PPP, which contain P2, exhibited significantly enhanced cell migration abilities, reaching more than five times that of the control group. This may be attributed to the porous structure of QTG@C@PPP and the support points provided by the short fibers, which facilitate cell migration, while P2 further promotes this effect.

3.13. Tube formation ability

Neovascularization is a crucial aspect of the wound healing process, where granulation tissue replaces necrotic skin tissue, with new blood vessels being essential components of granulation tissue. These new vessels provide oxygen, nutrients, and bioactive substances to the locally injured tissue, while also transporting metabolic waste, thus maintaining the stability of the microenvironment [54,55]. As shown in Fig. 8a, the number of new blood vessels in the QTG@C@PPP groups was significantly greater than that in the Blank group, and the morphology of the vessels was more regular. Statistical analysis (Fig. 8b–e) revealed that the number of blood vessel formations in the hydrogel-treated cells was more than double that of the Blank group. Other quantifiable indicators of angiogenesis, such as total tube length, number of segments, and junctions, also showed higher values in the QTG@PPP and QTG@C@PPP groups. This enhanced vascularization may be attributed to the presence of PTHR1 (parathyroid hormone receptor 1) on HUVEC. As a derivative of PTH, P2 stimulates the expression of eNOS and VEGF through the protein kinase A (PKA) and protein kinase C (PKC) pathways, promoting neovascularization [56,57]. Gel can also promote angiogenesis by upregulating the expression of CD31 and NF-κB, working synergistically with P2 [58].

3.14. Expression analysis of wound healing-related genes and proteins

Wound healing is complex process that requires not only neovascularization and fibrogenesis but also collagen deposition [59,60]. The treated expression of VEGF and CD31, which are related to vascular formation, as well as collagen deposition-related COL-1 expression and fibroblast growth factor FGF expression were assessed using qRT-PCR. As shown in Fig. 9a–d, the expression of these genes in the hydrogel group was upregulated, with the gene expression in QTG@PP group being over 1.3 times that of the Blank group. QTG@PPP and QTG@C@PPP groups showed even more significant regulation, with gene expression exceeding 2 times that of the Blank group.

This study also utilized immunofluorescence staining to investigate the expression of wound healing-related proteins in HUVEC, selecting genes consistent with those assessed by qRT-PCR. As shown in Fig. 9e, the red fluorescence intensity in cells treated with the various hydrogel groups was significantly stronger than that of the Blank group, with the QTG@C@PPP group exhibiting the most pronounced intensity compared to the other groups. Statistical analysis revealed (Fig. 9f–i) that the fluorescence intensity in each hydrogel group was over 1.4 times that of the Blank group, with the fluorescence intensity of CD31 and FGF in the QTG@C@PPP group being over 2.7 times that of the Blank group, while VEGF and COL-1 fluorescence intensity reached over 2.9 times that of the Blank group. Overall, wound healing-related genes and proteins in HUVEC were significantly upregulated by QTG@C@PPP. This may be attributed to the synergistic effects of the components within the hydrogel, particularly since P2 has been shown to promote the expression of wound healing-related genes [61,62].

3.15. In vivo wound healing

In vitro experiments have demonstrated that QTG@C@PPP exhibits good mechanical properties, excellent biocompatibility, antibacterial performance, and antioxidant capabilities. To evaluate the effect of QTG@C@PPP on diabetic wound healing in vivo, a diabetic rat model was first established, followed by the creation of a full-thickness skin injury model. As shown in Fig. 10a and b, the wound healing in the hydrogel group was better than that of Tegaderm^{3M} at all time points. On day 3, all wounds had formed initial scabs, with the hydrogel absorbing exudates from the wound surface and keeping the wound moist. By day 7, the wound areas in all groups had significantly decreased, the scabs had thickened, and there was almost no exudate observed. On day 14, the wounds treated with QTG@C@PPP were nearly closed, with some hair growth around the wound, and the closed wounds showed scar tissue. Analysis of the wound areas (Fig. 10c–e) revealed that QTG@PP had healed 10 % more wound area than

Tegaderm[3M] by day 3, while QTG@C@PPP had healed 62.8 % and 77.9 % of the wound area by days 3 and 7, respectively. Importantly, by day 14, the wound healing rate for QTG@C@PPP reached 96.2 %, nearly achieving complete healing, while the healing rate for Tegaderm[3M] was only 82.7 %. This result is similar to the in vivo result of the hydrogels used for diabetic wound repair, indicating that QTG@C@PPP also possesses strong abilities to promote diabetic wound healing in vivo [29,63]. This may be attributed to QTG@C@PPP maintaining moisture at the wound site during the initial healing phase and releasing Cel from the hydrogel, achieving a local anti-inflammatory effect. Additionally, the antibacterial effects of QCS and TA within the hydrogel facilitate a smooth transition to the mid-healing phase. During the mid-healing phase, P2 is continuously released from the core layer of the core-shell fibers, promoting the proliferation and migration of fibroblasts and endothelial cells, which leads to rapid formation of granulation and scar tissue. In the late healing phase, substantial collagen deposition and initial vascular formation occur, entering the tissue remodeling phase, ultimately leading to wound healing [35].

3.16. Histological analysis

Histological staining was used to further analyze the effects of QTG@C@PPP on diabetic wounds. As shown in Fig. 11a, by day 3, QTG@PPP and QTG@C@PPP exhibited thick and dense granulation tissue, while the Tegaderm[3M] only formed weak granulation tissue. By day 7, the epithelial layer of QTG@C@PPP began to thin in preparation for re-epithelialization, whereas the epithelial layers in the other groups remained relatively thick. By day 14, the wound treated with QTG@C@PPP was covered by newly formed epithelium, accompanied by the generation of blood vessels and hair follicles. According to the analysis in Fig. 11c, the rates of epidermal growth varied among the hydrogel groups on day 14. The Tegaderm[3M] and QTG@PP had not yet begun re-epithelialization, retaining a dense layer of granulation tissue. In contrast, QTG@C@PP had started re-epithelialization, resulting in a thinner epidermis. QTG@PPP showed a high degree of re-epithelialization, while QTG@C@PPP nearly completed epidermal regeneration, forming new blood vessels and hair follicles, resulting in the thickest epidermis.

Collagen fibers play a protective role for surrounding blood vessels and nerves, while also facilitating cell adhesion and growth [64]. As shown in Fig. 11b, the hydrogel groups exhibited greater collagen deposition at all time points, with QTG@C@PPP showing the highest levels. Statistical analysis of collagen density, illustrated in Fig. 11d–f, revealed that on day 3, the Tegaderm[3M] group had only 20 % collagen density, while QTG@C@PPP reached over 40 %. By day 7, the QTG@PP group showed 38 % collagen deposition, with the other hydrogel groups performing even better. By day 14, the Tegaderm[3M] group had a collagen density of 55.9 %, whereas QTG@C@PPP reached 81 %, indicating that QTG@C@PPP has the capability to enhance collagen deposition and promote the formation of tissue fibrous structures. P2 has been confirmed in previous studies by our research group to promote collagen deposition [26]. Gel, as the product of collagen, also has the ability to promote collagen regeneration. The two components synergistically enhance collagen formation within the wound [65].

3.17. Immunohistochemical analysis

To investigate the effects of QTG@C@PPP on inflammation and angiogenesis in diabetic wounds, immunohistochemical staining was performed on the wound healing tissue on day 14. As shown in Fig. 12a, both QTG@C@PP and QTG@C@PPP containing Cel significantly promoted the expression of the anti-inflammatory factor IL-4, while suppressing the expression of pro-inflammatory factors IL-6 and TNF-α. Statistical analysis revealed (Fig. 12b–d) that compared to the Tegaderm[3M], the expression level of IL-4 in the QTG@C@PPP group increased by 100 %, while the expression levels of IL-6 and TNF-α were reduced by half, indicating that the Cel carried in QTG@C@PPP was successfully released and acted locally at the wound site. Furthermore, each molecule of TA contains 10 catechol or gallic acid groups, providing strong radical-scavenging and anti-inflammatory effects [66]. QCS also has the ability to inhibit the production of IL-6, IL-8, and TNF-α, working synergistically with TA and Cel to achieve an anti-inflammatory effect [67,68]. VEGF was expressed the most in QTG@PPP and QTG@C@PPP containing P2, reaching 1.9 times that of the Tegaderm[3M] group, consistent with the in vitro experimental results. This indicates that QTG@C@PPP also has a strong capacity to promote angiogenesis in vivo.

4. Conclusion

In this work, a hydrogel containing core-shell fibers was developed as diabetic wound dressing. Inspired by the addition of fibers to adobes, electrospun fibers were incorporated into the hydrogel to enhance its mechanical properties, while the core-shell structure also endowed the material with sustained drug release capabilities. QTG@C@PPP exhibits tissue adhesion and maintain a moist wound environment through water absorption and retention, while also being injectable. QTG@C@PPP demonstrates good antibacterial and antioxidant properties, along with excellent biocompatibility that promotes cell proliferation and migration. Furthermore, in the diabetic full-thickness skin injury model, QTG@C@PPP exhibited strong ability to enhance wound healing and collagen deposition, while also demonstrating anti-inflammatory effects and promoting angiogenesis. In summary, QTG@C@PPP innovatively incorporates core-shell fibers into the hydrogel, achieving sustained release of P2 while enhancing the mechanical properties of the hydrogel. This provides a novel therapeutic approach for diabetic wound treatment and holds significant potential for advancing the development of composite materials combining hydrogels and electrospun fibers. Future research of QTG@C@PPP could explore the use of different drug combinations tailored to the specific conditions of wounds, such as combining antibiotics, hypoglycemic drugs, anti-inflammatory agents, and P2. Considering the unique microenvironment of diabetic wounds, developing rapid-responsive hydrogels that release drugs in response to specific triggers is another promising direction. Additionally, to reduce costs and align with effective regulatory frameworks, improving the production efficiency of core-shell fibers is also a key future goal of this study.

CRediT authorship contribution statement

Zouwei Li: Writing – review & editing, Writing – original draft, Methodology, Investigation, Data curation. **Renxin Chen:** Supervision, Project administration, Data curation, Conceptualization. **Zhuowen Hao:** Writing – review & editing, Investigation, Formal analysis. **Yan E:** Visualization, Validation, Formal analysis. **Qi Guo:** Validation, Investigation, Formal analysis. **Jingfeng Li:** Writing – review & editing, Writing – original draft, Supervision. **Shaobo Zhu:** Writing – review & editing, Funding acquisition, Conceptualization.

Declaration of competing interest

The authors declare that they have no known competing financial interests or personal relationships that could have appeared to influence the work reported in this paper.

Acknowledgements

The work was financially supported by the Key Research and Development Program of Hubei Province (2022BCA052) and the Key Research and Development Program of Wuhan City (2024020702030105). The authors thank Dr. Mingyuan Du from the Core Facility of Wuhan University for her assistance in FTIR analysis.

The authors thank Dr. Lili Dai and Dr. Wenting Fan from the Core Facility of Wuhan University for their technical support in SEM/EDS analysis.

Appendix A. Supplementary data

Supplementary data to this article can be found online at https://doi.org/10.1016/j.mtbio.2025.101477.

Data availability

Data will be made available on request.

References

[1] H. Sun, P. Saeedi, S. Karuranga, M. Pinkepank, K. Ogurtsova, B.B. Duncan, et al., IDF Diabetes Atlas: global, regional and country-level diabetes prevalence estimates for 2021 and projections for 2045, Diabetes Res. Clin. Pract. 183 (2022) 109–119.

[2] M. Chang, T.T. Nguyen, Strategy for treatment of infected diabetic foot ulcers, Acc. Chem. Res. 54 (5) (2021) 1080–1093.

[3] S.A. Castleberry, B.D. Almquist, W. Li, T. Reis, J. Chow, S. Mayner, et al., Self-assembled wound dressings silence MMP-9 and improve diabetic wound healing in vivo, Adv Mater 28 (9) (2016) 1809–1817.

[4] T. Dinh, F. Tecilazich, A. Kafanas, J. Doupis, C. Gnardellis, E. Leal, et al., Mechanisms involved in the development and healing of diabetic foot ulceration, DIABETES 61 (11) (2012) 2937–2947.

[5] C. Huang, L. Dong, B. Zhao, Y. Lu, S. Huang, Z. Yuan, et al., Anti-inflammatory hydrogel dressings and skin wound healing, Clin. Transl. Med. 12 (11) (2022) e1094.

[6] S. Cascone, G. Lamberti, Hydrogel-based commercial products for biomedical applications: a review, Int J Pharm 573 (2020) 118803.

[7] C. Huang, Z. Zhang, Y. Fang, K. Huang, Y. Zhao, H. Huang, et al., Cost-effective and natural-inspired lotus root/GelMA scaffolds enhanced wound healing via ROS scavenging, angiogenesis and reepithelialization, Int. J. Biol. Macromol. 278 (1) (2024) 134496.

[8] Z. Zhang, C. Huang, S. Guan, L. Wang, H. Yin, J. Yin, et al., Hybrid gelatin-ascorbyl phosphate scaffolds accelerate diabetic wound healing via ROS scavenging, angiogenesis and collagen remodeling, Biomater. Adv. 158 (2024) 213779.

[9] Y. Fang, T. Nie, G. Li, L. Wang, J. Du, J. Wu, Multifunctional antibiotic hydrogel doped with antioxidative lycopene-based liposome for accelerative diabetic wound healing, Chem Eng J 480 (2024) 147930.

[10] Y. Gao, L. Wang, C. Zhou, Y. Zhao, H. Huang, J. Wu, Low-dimensional antimicrobial nanomaterials in anti-infection treatment and wound healing, Chin. Chem. Lett. (2024) 110028.

[11] E. Barrett-Catton, M.L. Ross, P. Asuri, Multifunctional hydrogel nanocomposites for biomedical applications, POLYMERS-BASEL 13 (6) (2021).

[12] A. Luraghi, F. Peri, L. Moroni, Electrospinning for drug delivery applications: a review, J Control Release 334 (2021) 463–484.

[13] R. Chen, J. Wang, L. Chen, Z. Li, Q. Feng, F. Chen, et al., Electrospunned nanofiber membranes of PTH-related peptide loaded biopolymers for osteoporotic bone defect repair, Mater. Des. 244 (2024) 113179.

[14] Y. Lu, J. Huang, G. Yu, R. Cardenas, S. Wei, E.K. Wujcik, et al., Coaxial electrospun fibers: applications in drug delivery and tissue engineering, WIRES NANOMED NANOBI 8 (5) (2016) 654–677.

[15] M. Bazgir, W. Zhang, X. Zhang, J. Elies, M. Saeinasab, P. Coates, et al., Fabrication and characterization of PCL/PLGA coaxial and bilayer fibrous scaffolds for tissue engineering, Materials 14 (21) (2021) 6295.

[16] C. Chen, J. Tang, Y. Gu, L. Liu, X. Liu, L. Deng, et al., Bioinspired hydrogel electrospun fibers for spinal cord regeneration, Adv. Funct. Mater. 29 (4) (2019) 1806899.

[17] Caballero Caballero, Chinas Castillo, M. Bernabé, Alavéz Ramirez, S. Rivera, Effect on compressive and flexural strength of agave fiber reinforced adobes, J. Nat. Fibers 15 (4) (2018) 575–585.

[18] R. Ramkrishnan, M.R. Sruthy, A. Sharma, V. Karthik, Effect of random inclusion of sisal fibres on strength behavior and slope stability of fine grained soils, Mater Today: Proc 5 (11) (2018) 25313–25322.

[19] B. Niemczyk-Soczynska, A. Zaszczyńska, K. Zabielski, P. Sajkiewicz, Hydrogel, electrospun and composite materials for bone/cartilage and neural tissue engineering, Materials 14 (22) (2021).

[20] C. Xue, X. Xu, L. Zhang, Y. Liu, S. Liu, Z. Liu, et al., Self-healing/pH-responsive/inherently antibacterial polysaccharide-based hydrogel for a photothermal strengthened wound dressing, Colloid. Surface. B 218 (2022) 112738.

[21] B. Kaczmarek, Tannic acid with antiviral and antibacterial activity as A promising component of biomaterials-A minireview, Materials 13 (14) (2020) 3224.

[22] S.M. Ahsan, M. Thomas, K.K. Reddy, S.G. Sooraparaju, A. Asthana, I. Bhatnagar, Chitosan as biomaterial in drug delivery and tissue engineering, Int. J. Biol. Macromol. 110 (2018) 97–109.

[23] X. Yuan, Z. Zhu, P. Xia, Z. Wang, X. Zhao, X. Jiang, et al., Tough gelatin hydrogel for tissue engineering, Adv. Sci. 10 (24) (2023) e2301665.

[24] M.J. Ellis, J.B. Chaudhuri, Poly(lactic-co-glycolic acid) hollow fibre membranes for use as a tissue engineering scaffold, Biotechnol. Bioeng. 96 (1) (2007) 177–187.

[25] B. Zavan, C. Gardin, V. Guarino, T. Rocca, I. Cruz Maya, F. Zanotti, et al., Electrospun PCL-based vascular grafts: in vitro tests, NANOMATERIALS-BASEL 11 (3) (2021).

[26] L. Ang, H. Zhengzhe, L. Zongyue, L. Jingfeng, L. Xiaolin, Z. Zhichang, A PTHrP-2 loaded adhesive cellulose acetate nanofiber mat as wound dressing accelerates wound healing, Mater. Des. 212 (2021) 110241.

[27] J. Huang, D. Lin, Z. Wei, Q. Li, J. Zheng, Q. Zheng, et al., Parathyroid hormone derivative with reduced osteoclastic activity promoted bone regeneration via synergistic bone remodeling and angiogenesis, Small 16 (6) (2020) e1905876.

[28] L. Mude, S. Jupudi, A.K. Swaroop, V. Tallapaneni, V. Karri, Molecular insights in repurposing selective COX-2 inhibitor celecoxib against matrix metalloproteinases in potentiating delayed wound healing: a molecular docking and MMPB/SA based analysis of molecular dynamic simulations, J. Biomol. Struct. Dyn. 42 (5) (2024) 2437–2448.

[29] W. Zhou, Z. Duan, J. Zhao, R. Fu, C. Zhu, D. Fan, Glucose and MMP-9 dual-responsive hydrogel with temperature sensitive self-adaptive shape and controlled drug release accelerates diabetic wound healing, Bioact. Mater. 17 (2022) 1–17.

[30] S. Ge, N. Ji, S. Cui, W. Xie, M. Li, Y. Li, et al., Coordination of covalent cross-linked gelatin hydrogels via oxidized tannic acid and ferric ions with strong mechanical properties, J. Agric. Food Chem. 67 (41) (2019) 11489–11497.

[31] S. Guo, Y. Ren, R. Chang, Y. He, D. Zhang, F. Guan, et al., Injectable self-healing adhesive chitosan hydrogel with antioxidative, antibacterial, and hemostatic activities for rapid hemostasis and skin wound healing, ACS Appl. Mater. Interfaces 14 (30) (2022) 34455–34469.

[32] Y. Peng, Y. Ma, Y. Bao, Z. Liu, L. Chen, F. Dai, et al., Electrospun PLGA/SF/artemisinin composite nanofibrous membranes for wound dressing, Int. J. Biol. Macromol. 183 (2021) 68–78.

[33] L. Pan, J. Yang, L. Xu, Preparation and characterization of simvastatin-loaded PCL/PEG nanofiber membranes for drug sustained release, Molecules 27 (21) (2022) 7158.

[34] Z. Yang, R. Huang, B. Zheng, W. Guo, C. Li, W. He, et al., Highly stretchable, adhesive, biocompatible, and antibacterial hydrogel dressings for wound healing, Adv. Sci. 8 (8) (2021) 2003627.

[35] P.H. Wang, B.S. Huang, H.C. Horng, C.C. Yeh, Y.J. Chen, Wound healing, J. Chin. Med. Assoc. 81 (2) (2018) 94–101.

[36] S. Peng, A. Hu, J. Ai, W. Zhang, D. Wang, Changes in molecular structure of extracellular polymeric substances (EPS) with temperature in relation to sludge macro-physical properties, Water Res. 201 (2021) 117316.

[37] J. Wu, Z. Pan, Z.Y. Zhao, M.H. Wang, L. Dong, H.L. Gao, et al., Anti-swelling, robust, and adhesive extracellular matrix-mimicking hydrogel used as intraoral dressing, Adv Mater 34 (20) (2022) e2200115.

[38] Z. Liu, Z. Zhang, R.O. Ritchie, Structural orientation and anisotropy in biological materials: functional designs and mechanics, Adv. Funct. Mater. 30 (10) (2020) 1908121.

[39] I.A. Sogias, A.C. Williams, V.V. Khutoryanskiy, Why is chitosan mucoadhesive? Biomacromolecules 9 (7) (2008) 1837–1842.

[40] L. Li, H. Peng, Y. Du, H. Zheng, A. Yang, G. Lv, et al., An antibacterial biomimetic adhesive with strong adhesion in both dry and underwater situations, J. Mater. Chem. B 10 (7) (2022) 1063–1076.

[41] A. Ahmady, N.H. Abu Samah, A review: gelatine as a bioadhesive material for medical and pharmaceutical applications, Int J Pharm 608 (2021) 121037.

[42] C.K. Sen, S. Roy, S.S. Mathew-Steiner, G.M. Gordillo, Biofilm management in wound Care, Plast. Reconstr. Surg. 148 (2) (2021), 275e-88e.

[43] C. Xing, H. Zhu, X. Dou, L. Gao, S. Baddi, Y. Zou, et al., Infected diabetic wound regeneration using peptide-modified chiral dressing to target revascularization, ACS Nano 17 (7) (2023) 6275–6291.

[44] H. Tan, R. Ma, C. Lin, Z. Liu, T. Tang, Quaternized chitosan as an antimicrobial agent: antimicrobial activity, mechanism of action and biomedical applications in orthopedics, Int. J. Mol. Sci. 14 (1) (2013) 1854–1869.

[45] D. Jakub, S. Małgorzata, K. Ewa, K. Małgorzata, D. Anna, D. Bartłomiej, et al., Glutathione peroxidase (GPx) and superoxide dismutase (SOD) activity in patients with diabetes mellitus type 2 infected with Epstein-Barr virus, PLoS One 15 (3) (2020) e0230374.

[46] D. Liling, D. Chenzhen, S. Peiyang, C. Tianyi, R. Shunli, A.D. G, et al., The role of oxidative stress and antioxidants in diabetic wound healing, Oxid. Med. Cell. Longev. 2021 (2021) 8852759.

[47] S. Guo, M. Yao, D. Zhang, Y. He, R. Chang, Y. Ren, et al., One-step synthesis of multifunctional chitosan hydrogel for full-thickness wound closure and healing, Adv Healthc Mater 11 (4) (2022) e2101808.

[48] N.S. Khan, A. Ahmad, S.M. Hadi, Anti-oxidant, pro-oxidant properties of tannic acid and its binding to DNA, Chem. Biol. Interact. 125 (3) (2000) 177–189.

[49] Y. Ji, J. Lin, R. Liu, K. Wang, M. Chang, Z. Gao, et al., Celecoxib attenuates hindlimb unloading-induced muscle atrophy via suppressing inflammation, oxidative stress and ER stress by inhibiting STAT3, Inflammopharmacology 32 (2) (2024) 1633–1646.

[50] H.-Y. Lin, C.-C. Chou, Antioxidative activities of water-soluble disaccharide chitosan derivatives, Food Res. Int. 37 (9) (2004) 883–889.

[51] A. Sivanantham, D. Pattarayan, R. Bethunaickan, A. Kar, S.K. Mahapatra, R. K. Thimmulappa, et al., Tannic acid protects against experimental acute lung injury through downregulation of TLR4 and MAPK, J. Cell. Physiol. 234 (5) (2019) 6463–6476.

[52] Y. Wang, Z. Cao, Q. Wei, K. Ma, W. Hu, Q. Huang, et al., VH298-loaded extracellular vesicles released from gelatin methacryloyl hydrogel facilitate diabetic wound healing by HIF-1α-mediated enhancement of angiogenesis, Acta Biomater. 147 (2022) 342–355.

[53] L. He, C. Zhu, J. Jia, X.Y. Hao, X.Y. Yu, X.Y. Liu, et al., ADSC-Exos containing MALAT1 promotes wound healing by targeting miR-124 through activating Wnt/β-catenin pathway, Biosci. Rep. 40 (5) (2020).
[54] V. Falanga, Wound healing and its impairment in the diabetic foot, Lancet (N. Am. Ed.) 366 (9498) (2005) 1736–1743.
[55] J.T. Wyffels, L.E. Edsberg, Granulation tissue of chronic pressure ulcers as a predictive indicator of wound closure, Adv. Skin Wound Care 24 (10) (2011) 464–473.
[56] G. Rashid, J. Bernheim, J. Green, S. Benchetrit, Parathyroid hormone stimulates the endothelial expression of vascular endothelial growth factor, Eur. J. Clin. Invest. 38 (11) (2008) 798–803.
[57] G. Rashid, J. Bernheim, J. Green, S. Benchetrit, Parathyroid hormone stimulates the endothelial nitric oxide synthase through protein kinase A and C pathways, Nephrol. Dial. Transplant. 22 (10) (2007) 2831–2837.
[58] Y. Mizuno, T. Taguchi, A hydrophobic gelatin fiber sheet promotes secretion of endogenous vascular endothelial growth factor and stimulates angiogenesis, RSC Adv. 10 (42) (2020) 24800–24807.
[59] L. Gardeazabal, A. Izeta, Elastin and collagen fibres in cutaneous wound healing, EXP DERMATOL 33 (3) (2024) e15052.
[60] P. Bainbridge, Wound healing and the role of fibroblasts, J. Wound Care 22 (8) (2013), 407-8, 10-12.
[61] R. Kashimoto, Y. Kamei, S. Nonaka, Y. Kondo, S. Yamamoto, S. Furukawa, et al., FGF signaling induces the regeneration of collagen fiber structure during skin wound healing in axolotls, Dev. Biol. 498 (2023) 14–25.
[62] Y.F. Shen, J.H. Huang, K.Y. Wang, J. Zheng, L. Cai, H. Gao, et al., PTH Derivative promotes wound healing via synergistic multicellular stimulating and exosomal activities, Cell Commun. Signal. 18 (1) (2020) 40.
[63] Y. Xiong, L. Chen, P. Liu, T. Yu, C. Lin, C. Yan, et al., All-in-One: multifunctional hydrogel accelerates oxidative diabetic wound healing through timed-release of exosome and fibroblast growth factor, Small 18 (1) (2022) e2104229.
[64] S. Chattopadhyay, R.T. Raines, Review collagen-based biomaterials for wound healing, Biopolymers 101 (8) (2014) 821–833.
[65] M. Shi, Y. Gao, L. Lee, T. Song, J. Zhou, L. Yan, et al., Adaptive gelatin microspheres enhanced stem cell delivery and integration with diabetic wounds to activate skin tissue regeneration, Front. Bioeng. Biotechnol. 10 (2022) 813805.
[66] J. Yeo, J. Lee, S. Yoon, W.J. Kim, Tannic acid-based nanogel as an efficient anti-inflammatory agent, Biomater. Sci. 8 (4) (2020) 1148–1159.
[67] S.H. Liu, Y.H. Chang, M.T. Chiang, Chitosan reduces gluconeogenesis and increases glucose uptake in skeletal muscle in streptozotocin-induced diabetic rats, J. Agric. Food Chem. 58 (9) (2010) 5795–5800.
[68] I.M. Fang, C.H. Yang, C.M. Yang, Chitosan oligosaccharides attenuate ocular inflammation in rats with experimental autoimmune anterior uveitis, Mediators Inflamm 2014 (2014) 827847.